Geophysical Framework Based on Analysis of Aeromagnetic and Gravity Data, Verde River Headwaters, North-Central Arizona

By V.E. Langenheim, Ed DeWitt, and Laurie Wirt

Chapter C

Geologic Framework of Aquifer Units and Ground-Water Flowpaths, Verde River Headwaters, North-Central Arizona

Edited by Laurie Wirt, Ed DeWitt, and V.E. Langenheim

Prepared in cooperation with the Arizona Water Protection Fund Commission

Open-File Report 2004–1411-C

U.S. Department of the Interior
U.S. Geological Survey

U.S. Department of the Interior
Gale A. Norton, Secretary

U.S. Geological Survey
P. Patrick Leahy, Acting Director

U.S. Geological Survey, Reston, Virginia: 2005

For product and ordering information:
World Wide Web: http://www.usgs.gov/pubprod
Telephone: 1-888-ASK-USGS

For more information on the USGS--the Federal source for science about the Earth, its natural and living resources, natural hazards, and the environment:
World Wide Web: http://www.usgs.gov
Telephone: 1-888-ASK-USGS

Suggested citation:
Langenheim, V.E., DeWitt, E., and Wirt, L., 2005, Geophysical Framework Based on Analysis of Aeromagnetic and Gravity Data, Verde River Headwaters, North-Central Arizona: *in* Wirt, Laurie, DeWitt, Ed, and Langenheim, V.E., eds., Geologic Framework of Aquifer Units and Ground-Water Flowpaths, Verde River Headwaters, North-Central Arizona: U.S. Geological Survey Open-File Report 2004-1411-C, 25 p.

Contents

Abstract 1
Introduction 1
    Acknowledgments 1
Data and Methods 1
    Aeromagnetic and Gravity Data 1
    Filtering Techniques 3
        Wavelength Separation 3
        Geophysical Boundaries 3
    Drill Holes and Physical Properties 3
    Geophysical Anomalies 14
    Depth to Basement Method 15
Results 16
    Depth to Basement 16
    Playa Deposit/Alluvial Fans 22
    Distribution of Volcanic Rocks in Subsurface 22
Conclusions and Recommendations 24
References Cited 24

Figures

C1. Shaded-relief topographic map of study area 2
C2. Aeromagnetic (reduced to pole) map of the study area 4
C3. Isostatic gravity 5
C4a. Aeromagnetic filtered bandpass-filtered to enhance shallow sources 6
C4b. Aeromagnetic field bandpass-filtered to enhance deep sources 7
C5. First vertical derivative of the magnetic field 8
C6. Aeromagnetic field filtered to enhance shallow sources 9
C7. Filtered gravity field to enhance shallow sources 10
C8. Pseudogravity map of the study area 11
C9. Density and magnetic boundaries 12
C10. Average densities of Tertiary sedimentary rocks derived from various methods 15
C11. Schematic representation of basin-basement separation 16
C12a. Thickness of Cenozoic sedimentary and volcanic fill using the density-depth function of Tucci and others (1982) 18
C12b. Thickness of Cenozoic sedimentary and volcanic fill using a density-depth function derived from resistivity logs 19
C13. Mismatch between basin thickness encountered in wells that did not encounter pre-Cenozoic bedrock and predicted basin thickness from the gravity inversion 20
C14. Basement gravity (Model 2) based on density-depth function derived from resistivity 21
C15. Interpretive map of study area. Geology on shaded-relief topography with magnetic boundaries ..... (oversized)

Tables

C1. Densities (g/cm^3) and magnetic susceptibilites (10^{-3} cgs units).....13
C2. Density-depth function 16

Geophysical Framework Based on Analysis of Aeromagnetic and Gravity Data

By V.E. Langenheim, Ed DeWitt, and Laurie Wirt

Abstract

Analysis of aeromagnetic and gravity data provides new insights on the geometry of geologic structures in the Verde River headwaters region. Magnetic anomalies reveal hidden volcanic rocks lying at shallow depths beneath the ground surface. For example, semicircular magnetic lows can be used to map the extent of shallowly buried (less than 200—300 meters) lati-andesite plugs. In contrast, Tertiary basalts produce worm-like anomaly patterns. The geophysical data also can be used to detect concealed faults within the study area. The Big Chino fault has the largest amount of vertical throw of any fault in the study area based on gravity, magnetic, and limited well data. The pervasive magnetic grain within Little Chino Valley is northeast- and northwest-striking, but apparently none of the structures responsible for this grain appear to have large vertical offsets like the Big Chino fault. Gravity data indicate 1—2 kilometers of basin fill beneath Big Chino Valley. Based on gravity inversions for basin thickness, the volume of total sediment in Big Chino Valley within the study area is estimated to be 140.2 to 158.4 cubic kilometers (1.14 to 1.29 x 10^8 acre-feet). The areal extent of the Big Chino gravity low coincides with a thick playa deposit delineated by analysis of well data. The lack of a distinct gravity low in Little Chino Valley suggests that the sedimentary and volcanic fill is much thinner (less than 1 kilometer) than that of Big Chino Valley.

Introduction

The goal of this geophysical study is to improve understanding of the subsurface geologic framework of the Verde River headwaters region (fig. C1). This work builds upon two earlier studies (Ostenaa and others, 1993; Water Resource Associates, 1989) that compiled well data and collected profiles of geophysical data. This study includes a more quantitative and detailed interpretation of aeromagnetic and gravity data collected by the U.S. Geological Survey in 1999—2000 than that presented in Langenheim and others (2000). The emphasis of this chapter is analysis of aeromagnetic and gravity data and how these data provide information on the geometry of geologic structures in the study area. Radiometric data are more useful for mapping surficial deposits and thus are discussed in Chapter B. The first part of the chapter deals with data methods, analysis, and description; the second part emphasizes the interpretation of the data; their hydrogeologic significance will be discussed in Chapter D.

The aeromagnetic data can be used to detect Tertiary volcanic rocks and certain rock types within the Proterozoic crystalline basement. The gravity data reflect the density contrast between basin sediments and pre-Cenozoic bedrock and density contrasts within the Proterozoic crystalline basement rocks. The analysis of these datasets is an effective tool in defining hidden structures important to ground-water studies, such as the configuration and structural fabric of basement and volcanic rocks beneath Tertiary sedimentary deposits.

Acknowledgments

We would like to thank the Arizona Water Protection Fund Commission for financial support (Arizona Water Protection Fund Grant 99-078). We appreciate the helpful comments of reviewers Tom Hildenbrand and Bob Jachens (U.S. Geological Survey, Menlo Park, Calif.), John Hoffmann (U.S. Geological Survey, Tucson, Ariz.) and Frank Corkhill (Arizona Dept. of Water Resources).

Data and Methods

Aeromagnetic and Gravity Data

Details of the processing techniques of the high-resolution aeromagnetic (and radiometric) data collected for the study are given in Langenheim and others (2000). Flight lines were oriented east-west, spaced 150 meters (.093 mile) apart, and flown at a nominal altitude of 150 meters (500 feet) above terrain, or as low as permitted by the Federal Aviation Administration and safety considerations. North-south control lines were spaced 3.0 kilometers (1.83 miles) apart. Total flight distance was 5,600 kilometers (3,480 miles). To shift anomalies over their respective sources, the magnetic data were reduced to the pole (fig. C2; Blakely, 1996). Accuracy of the data is estimated to be on the order of 0.5 to 1 nanoTesla (nT).

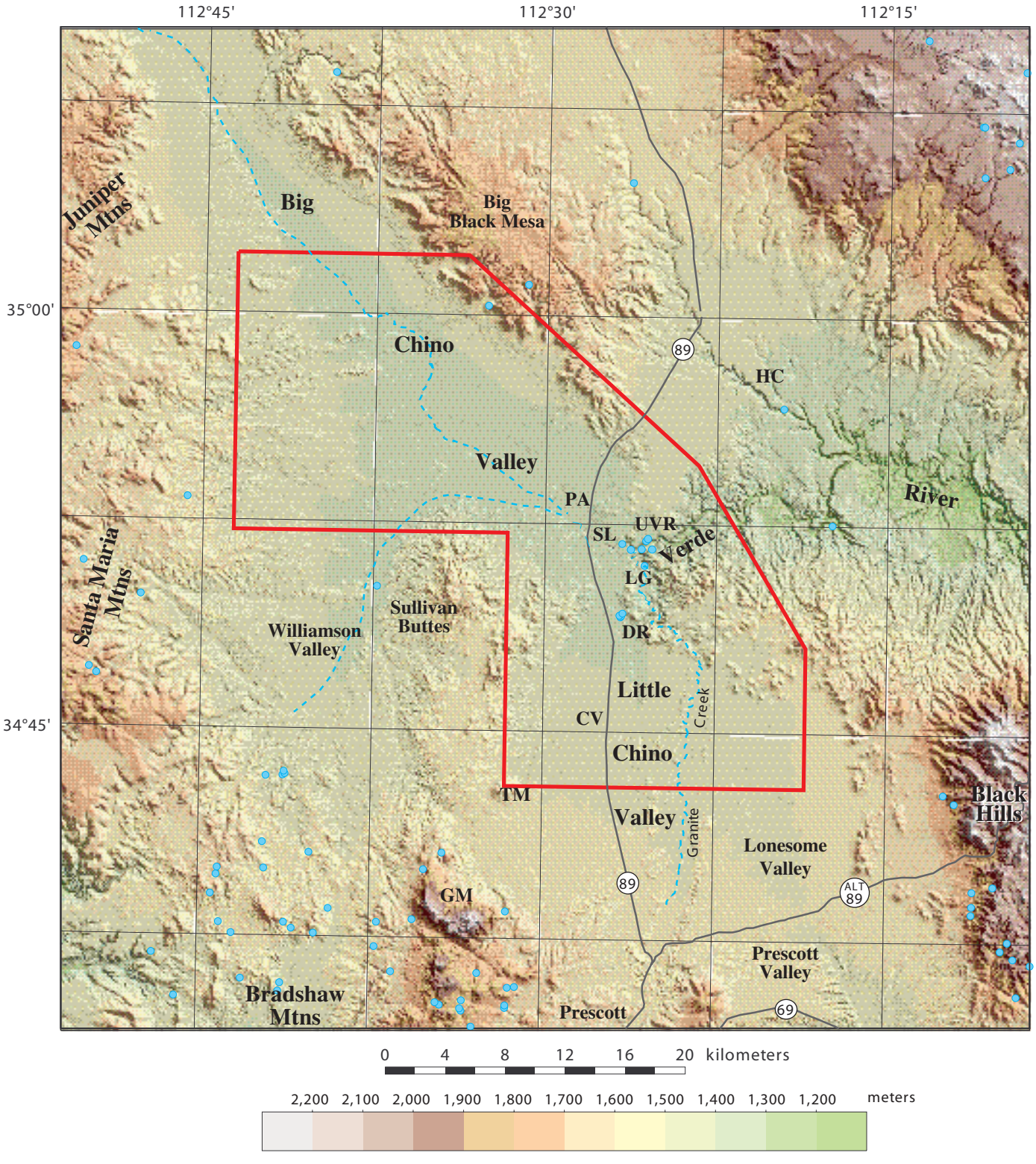

Figure C1. Shaded-relief topographic map of the study area. Aeromagnetic survey boundary is shown in red. Blue circles are spring locations. Dashed blue lines, ephemeral streams. UVR, upper Verde River springs; CV, town of Chino Valley; DR, Del Rio springs; GM, Granite Mountain; HC, Hell Canyon; LG, lower Granite Spring; PA, Paulden; SL, Sullivan Lake, TM, Table Mountain. Illumination direction from the northeast.

About 1,160 gravity stations were used to produce an isostatic gravity map of the region (Langenheim and others, 2000; Water Resource Associates, 1989). The isostatic gravity data reflect density variations within the middle and upper crust (fig. C3; Simpson and others, 1986). Details on the processing of these data are given in Langenheim and others (2000). Gravity stations are nonuniformly distributed in the region (fig. C3). Station spacing is on average one station per 2 cubic kilometers, although the station spacing is as low as one station per 10 cubic kilometers even within parts of the Big Chino and Little Chino Valleys. Accuracy of the data is estimated to be on the order of 0.1 to 0.5 milligal (mGal).

Filtering Techniques

Magnetic and gravity anomalies are produced by a variety of sources that range in size and depth. Superposition of anomalies from multiple sources can result in interpretational ambiguities. For example, both Proterozoic crystalline and Tertiary volcanic rock types are magnetic, but they are characterized by different anomaly wavelengths. Shallow sources typically cause short-wavelength anomalies, whereas deep sources cause long-wavelength anomalies. Generally, Tertiary volcanic rocks, which are comparatively thinner and shallower than Proterozoic crystalline rock, should produce shorter-wavelength anomalies. Several analytical techniques were applied to the geophysical data to enhance particular anomaly characteristics, such as wavelength or trend.

Wavelength Separation

To emphasize both short-wavelength anomalies caused by shallow sources (for example, Tertiary volcanic rock) and long-wavelength anomalies (for example, Proterozoic crystalline rock), a match filter was applied (Phillips, 2001). Match filtering separates the data into different wavelength components by modeling the observed spectra using two distinct equivalent source layers at increasing depths (see Phillips, 2001). Figures C4a and C4b show the resulting separated fields produced by the dipole equivalent-source layers at 0.320 kilometer and 3.88 kilometers depth, associated with shallow and deep sources, respectively. Another method, the first vertical derivative of the magnetic data (fig. C5) suppresses longer-wavelength trends caused by more deeply buried magnetic rock types (Blakely, 1996). A third method to sharpen the effects of near-surface sources involves analytically upward continuing the magnetic or gravity field by a small interval (100 meters for the magnetic data; 1 kilometer for the gravity data because of the nonuniform distribution of gravity stations). The method of upward continuation is the transformation of magnetic or gravity data measured on one surface to data that would be measured on a higher surface; this operation tends to smooth the data by attenuation of short-wavelength anomalies (Dobrin and Savit, 1988). This smoothed field then is subtracted from the unfiltered field to produce a residual field. The unfiltered and residual fields (figs. C2, C4, and C6 for the magnetic field; figs. C3 and C7 for the gravity field) illustrate the effectiveness of this approach to highlight subtle geologic features.

To help emphasize the more voluminous magnetic sources (such as those residing in the Proterozoic crystalline basement), the aeromagnetic anomalies are mathematically transformed into pseudogravity (or magnetic potential) anomalies (Baranov, 1957). This procedure effectively converts the magnetic field to the "gravity" field that would be produced if all magnetic material were replaced by proportionately dense material. The transformation (a) removes the dipolar effect of the magnetic field, thereby shifting the anomalies to a position directly over their sources, and (b) amplifies the long-wavelength features at the expense of short-wavelength anomalies (Blakely, 1996). The pseudogravity map is not independent of the map of the magnetic field, but simply a filtered rendition of the magnetic field that emphasizes long-wavelength anomalies (fig. C8).

Geophysical Boundaries

To help delineate structural trends and gradients expressed in the gravity field, a computer algorithm is used to locate the maximum horizontal gravity gradient (Blakely and Simpson, 1986; fig. C9). Gradient maxima occur approximately over vertical or near-vertical contacts that separate rocks of contrasting densities. For moderate to steep dips (45 degrees to vertical), the horizontal displacement of a gradient maximum from the top edge of an offset horizontal layer is always less than or equal to the depth to the top of the source (Grauch and Cordell, 1987). Magnetization boundaries (fig. C9) were calculated in a similar way as described in Blakely and Simpson (1986), by using the pseudogravity field produced from the residual magnetic field shown in figure C6.

Drill Holes and Physical Properties

Most of the drill holes in the study area are shallow (less than 100 meters) and do not have detailed or reliable lithologic logs. Well logs can provide critical geologic constraints needed in geophysical modeling and interpretation, but uncertainties in well log data quality limit their utility. This analysis used most of the well logs compiled by Krieger (1965) and Ostenaa and others (1993), augmented by well logs obtained from the Arizona Department of Water Resources (unpublished data). Figure C6 shows locations of utlized wells and illustrates their relatively uneven areal distribution.

Magnetic and gravity data reflect the subsurface distribution of magnetization and density. Magnetization (emu/cm^3) is the sum of induced and remanent components. The induced component depends on magnetic susceptibility (cgs unit) that is easily measured in the field. Magnetic susceptibility and density information of exposed rock types is critical to determine the sources of gravity and magnetic anomalies. Table C1

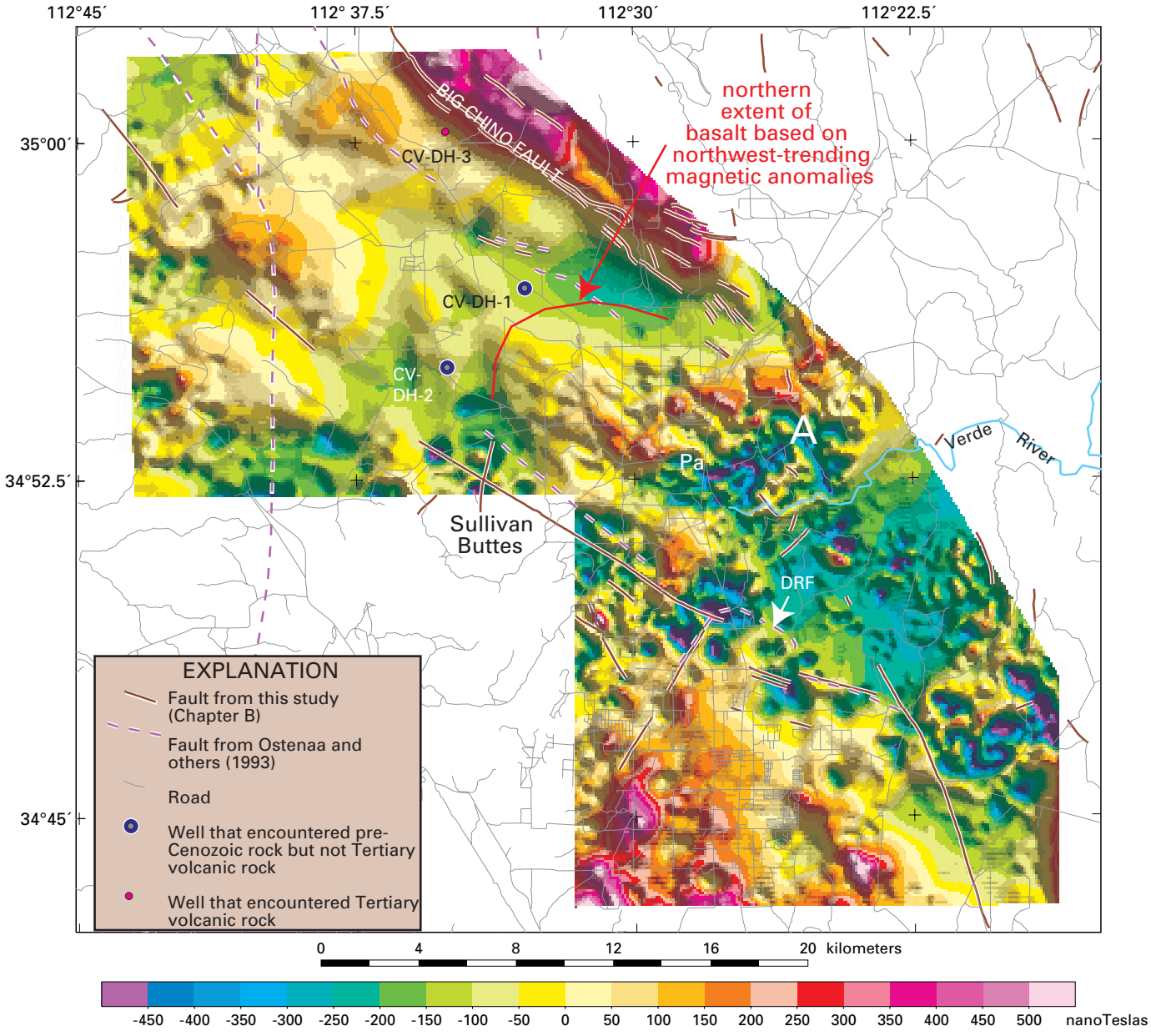

Figure C2. Aeromagnetic (reduced to pole) map of the study area. Anomalies are located over their sources if remanent magnetization is absent. "A" is an example of "worm-like" magnetic anomoly pattern produced by Tertiary basalt. DRF, Del Rio fault; Pa, Paulden.

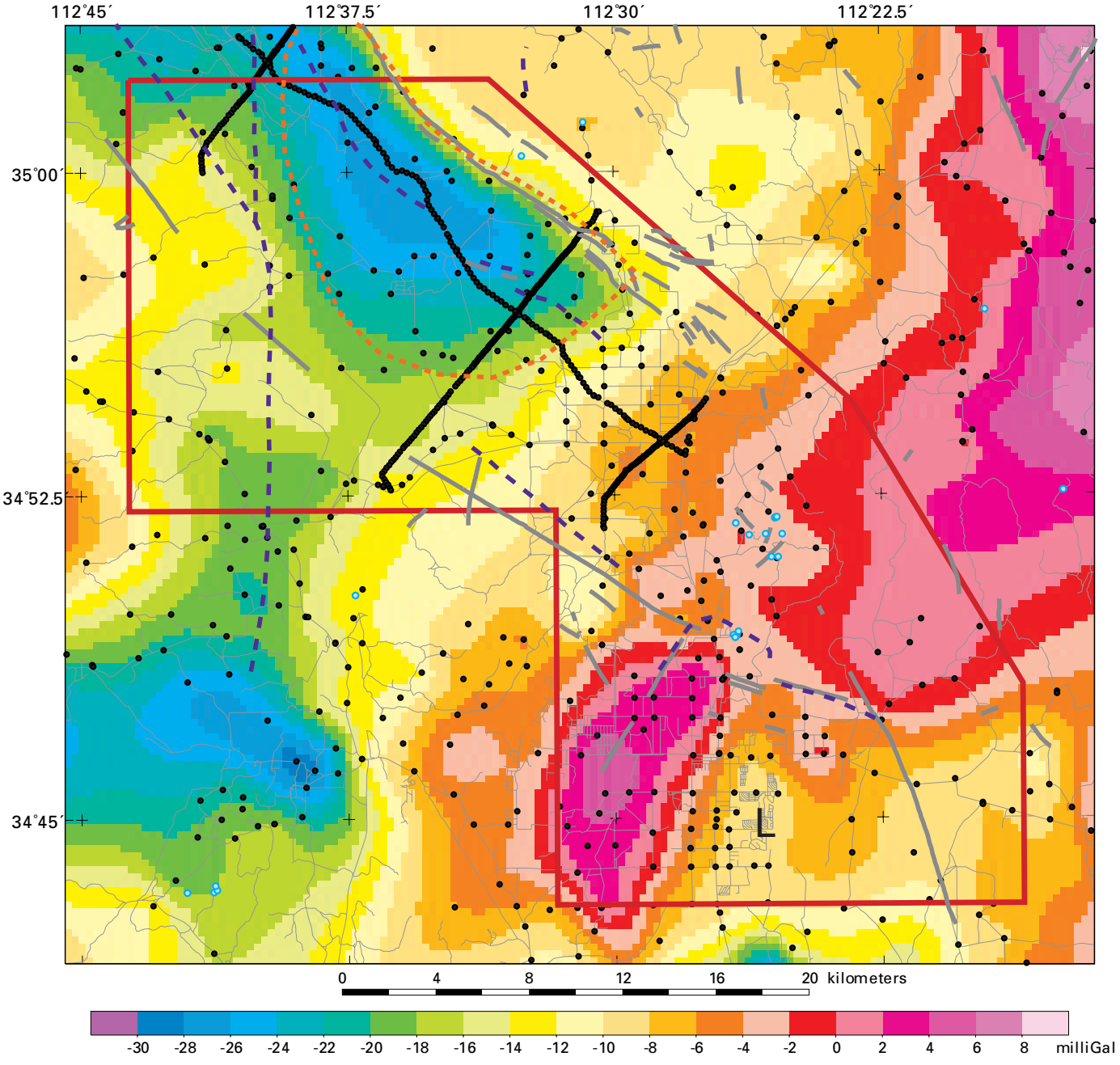

Figure C3. Isostatic gravity map. Black circles are gravity stations. Thick red line marks extent of aeromagnetic survey. Dashed orange line is approximate extent of the playa deposit that was interpreted as a clay deposit by Schwab (1995). Dark gray lines are faults determined in this study (Chapter B); dashed purple lines, faults from Ostenaa and others (1993). Blue circles are springs. "L" is small gravity low west of Granite Creek.

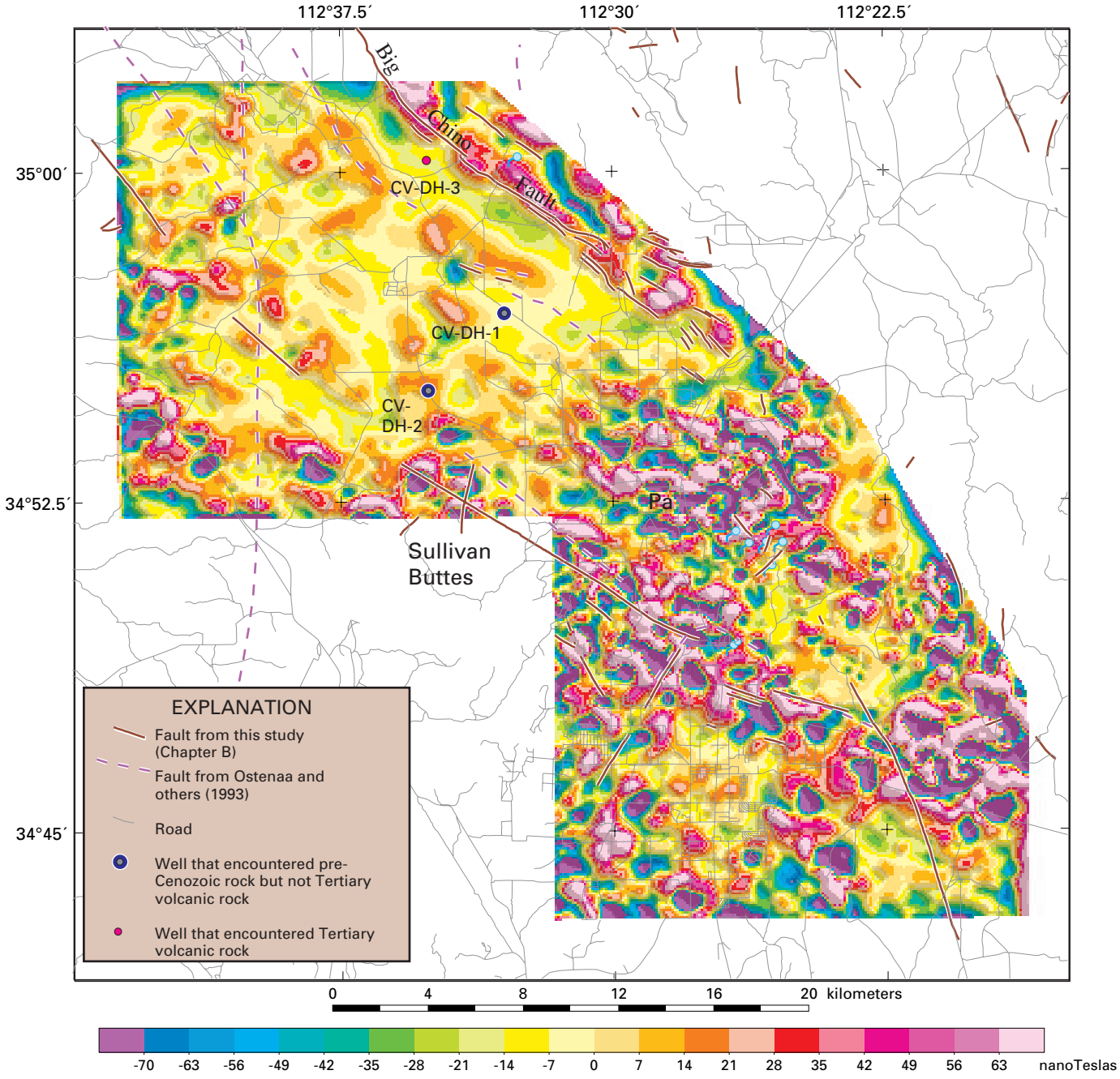

Figure C4a. Map of aeromagnetic field bandpass-filtered to enhance shallow sources (most lying <1km). Springs shown as blue circles with tails. Pa, Paulden.

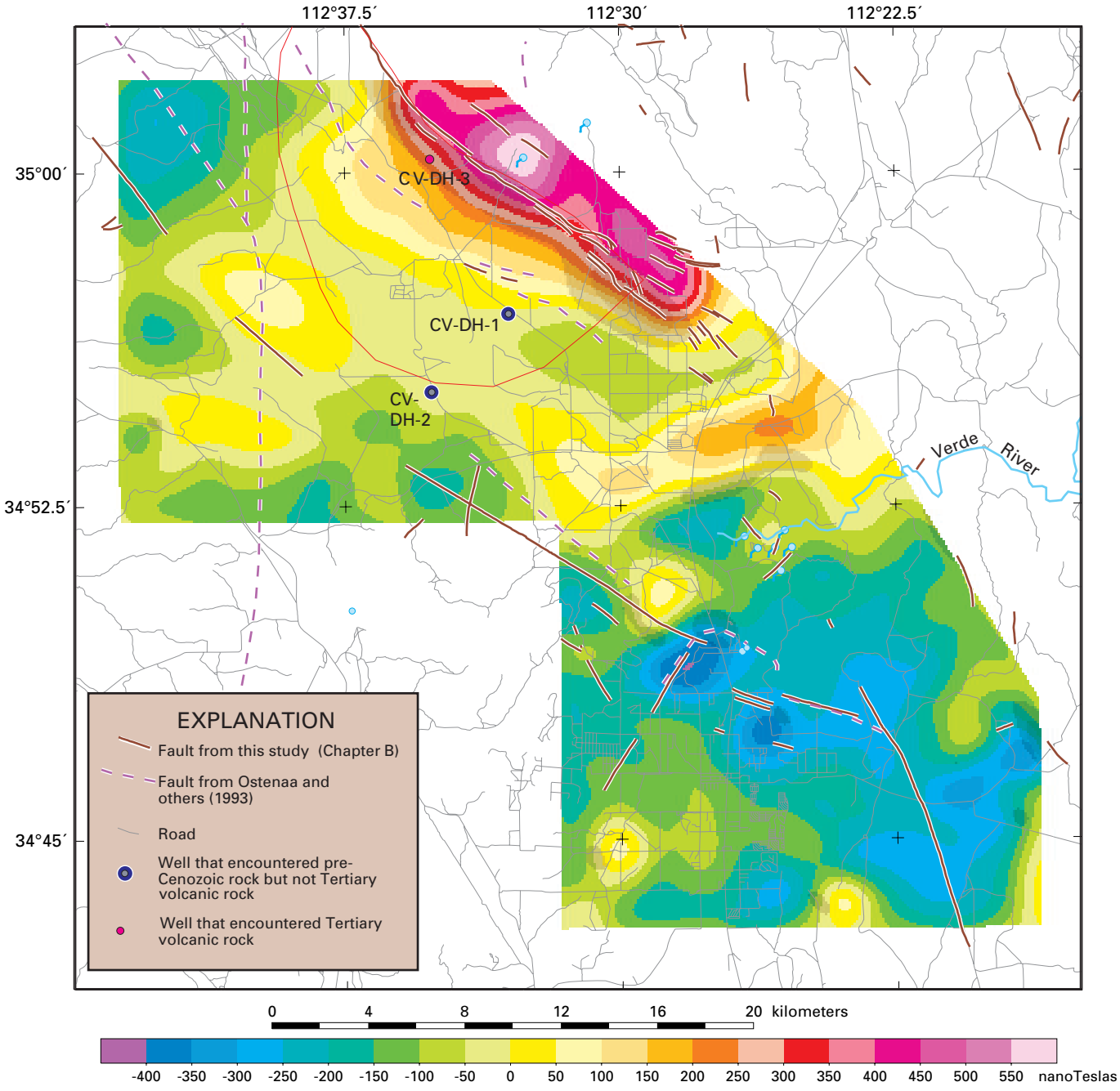

Figure C4b. Map of aeromagnetic field bandpass-filtered to enhance deep (approximately greater than 1-2 km) sources.

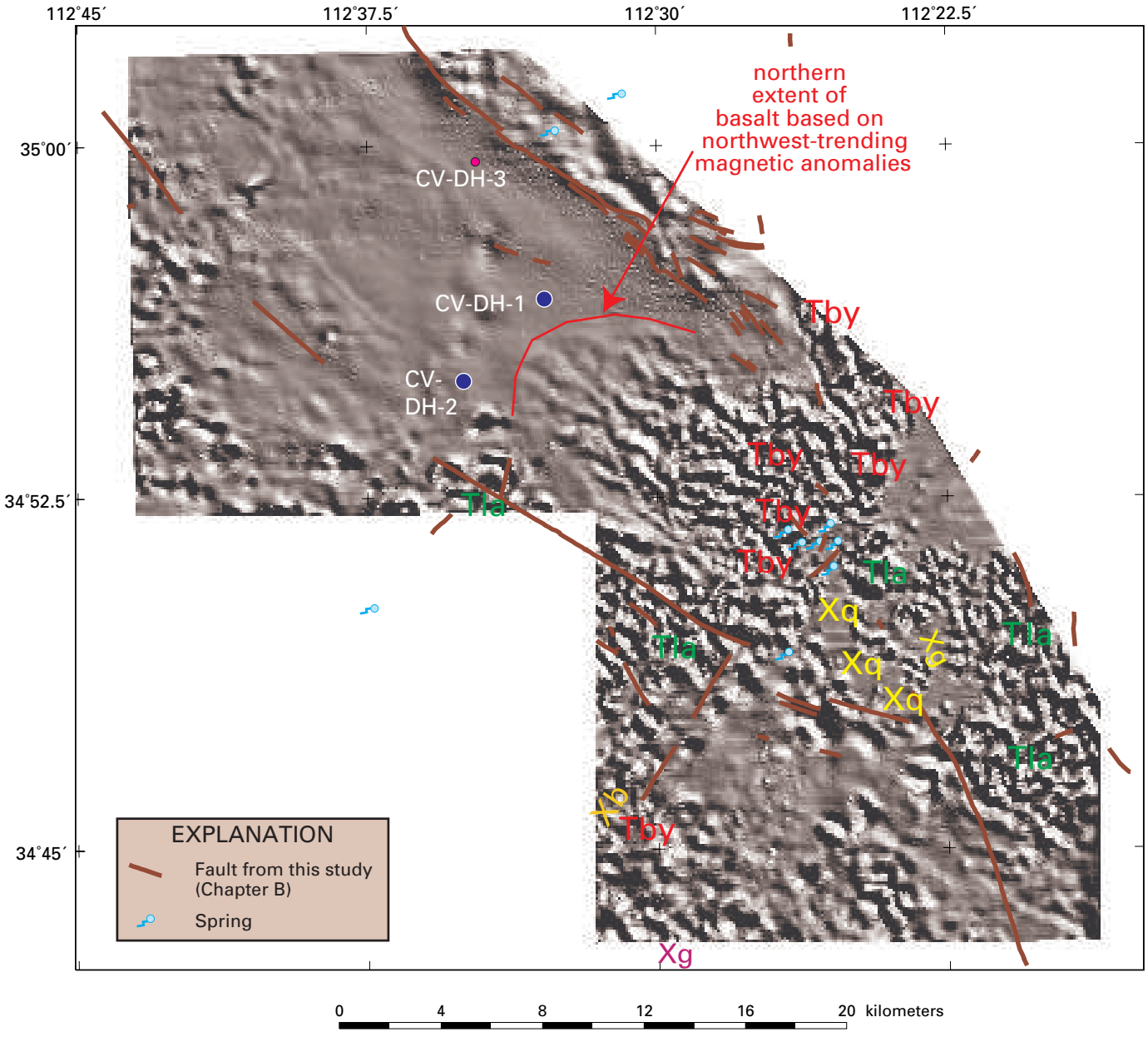

Figure C5. Map of first vertical derivative of the magnetic field. Xq, Xg, and Xb are exposed Proterozoic quartzite, granite and metabasalt, respectively; Tby, Tertiary basalt; Tla, Tertiary lati-andesite.

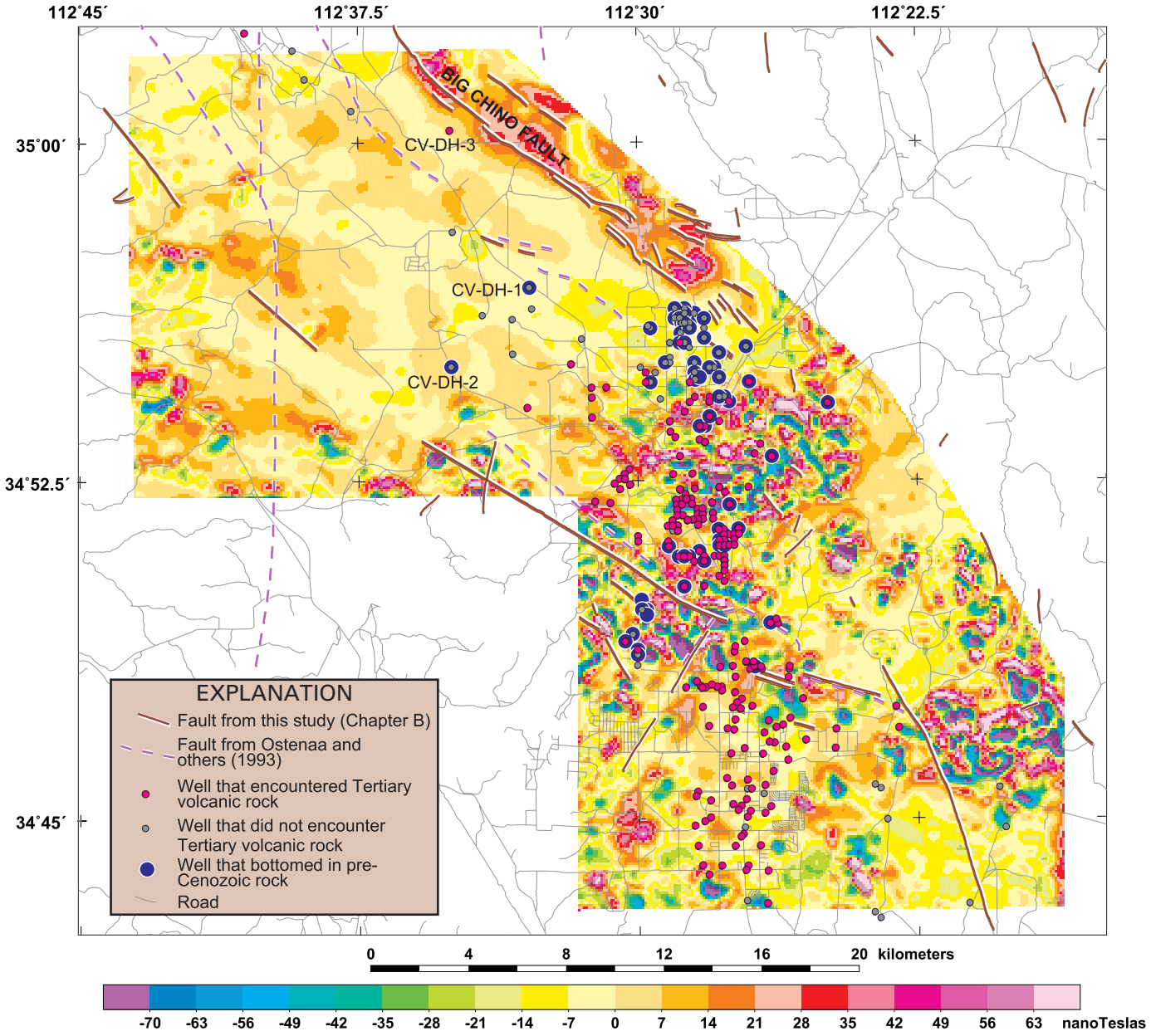

Figure C6. Map of aeromagnetic field filtered (by subtraction of upward continuation of magnetic field) to enhance shallow sources. Wells are from Krieger (1965), Ostenaa and others (1993), and ADWR unpublished data. Note that wells that did not encounter Tertiary volcanic rock may have been too shallow to encounter Tertiary volcanic rock; only those wells that bottom in pre-Cenozoic rock without penetrating Tertiary volcanic rock indicate an absence of Tertiary volcanic rock at that location.

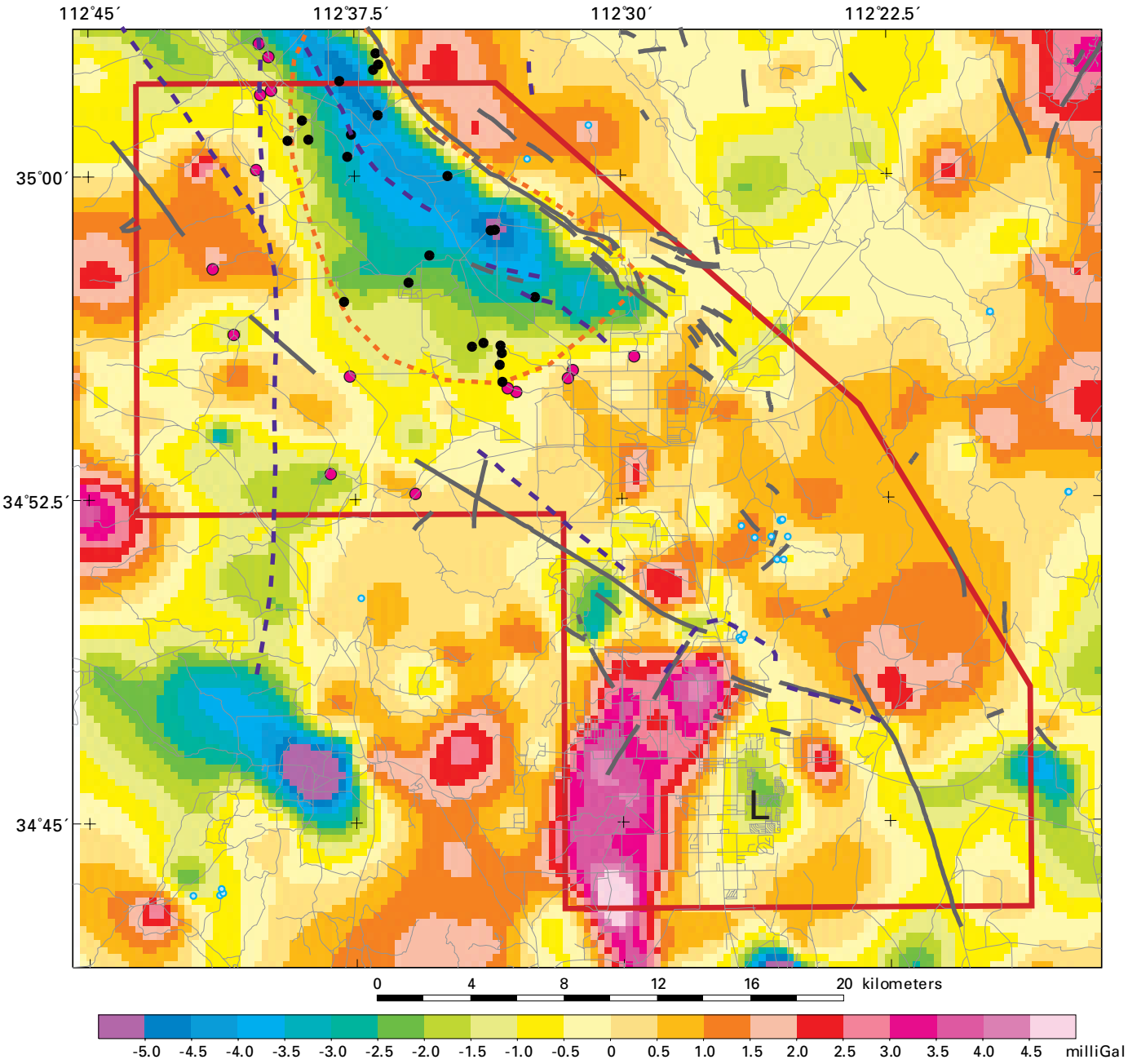

Figure C7. Map of filtered gravity field to enhance shallow sources. See Figure C3 caption for explanation of map. Black circles are wells within the playa deposit, magenta circles are wells around perimeter of playa deposit (from Schwab, 1995). "L" is small gravity low west of Granite Creek.

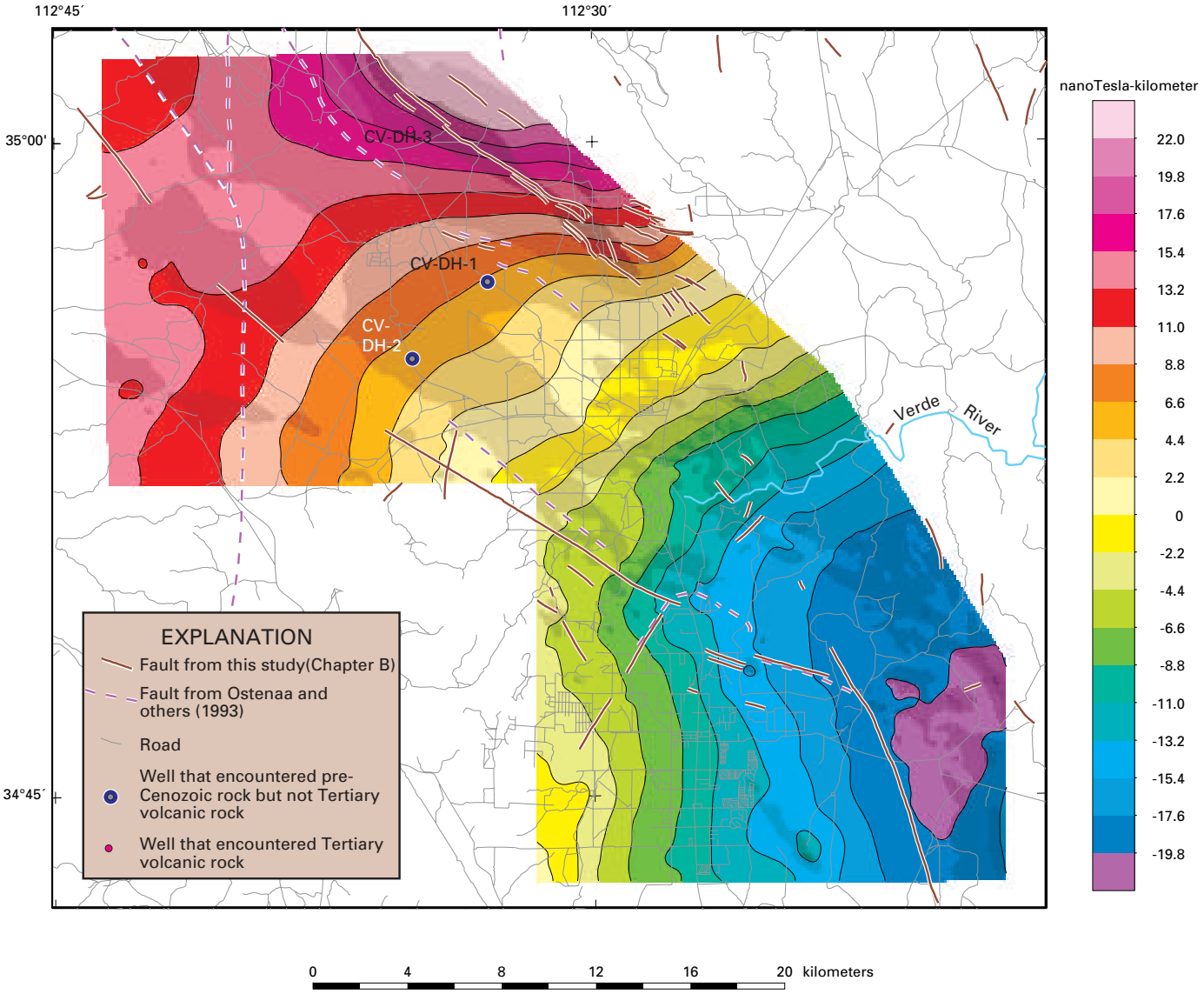

Figure C8. Shaded-relief pseudogravity map of the study area. The map emphasizes longer-wavelength anomalies (such as those residing in the Proterozoic crystalline basement). Illumination direction from the northeast.

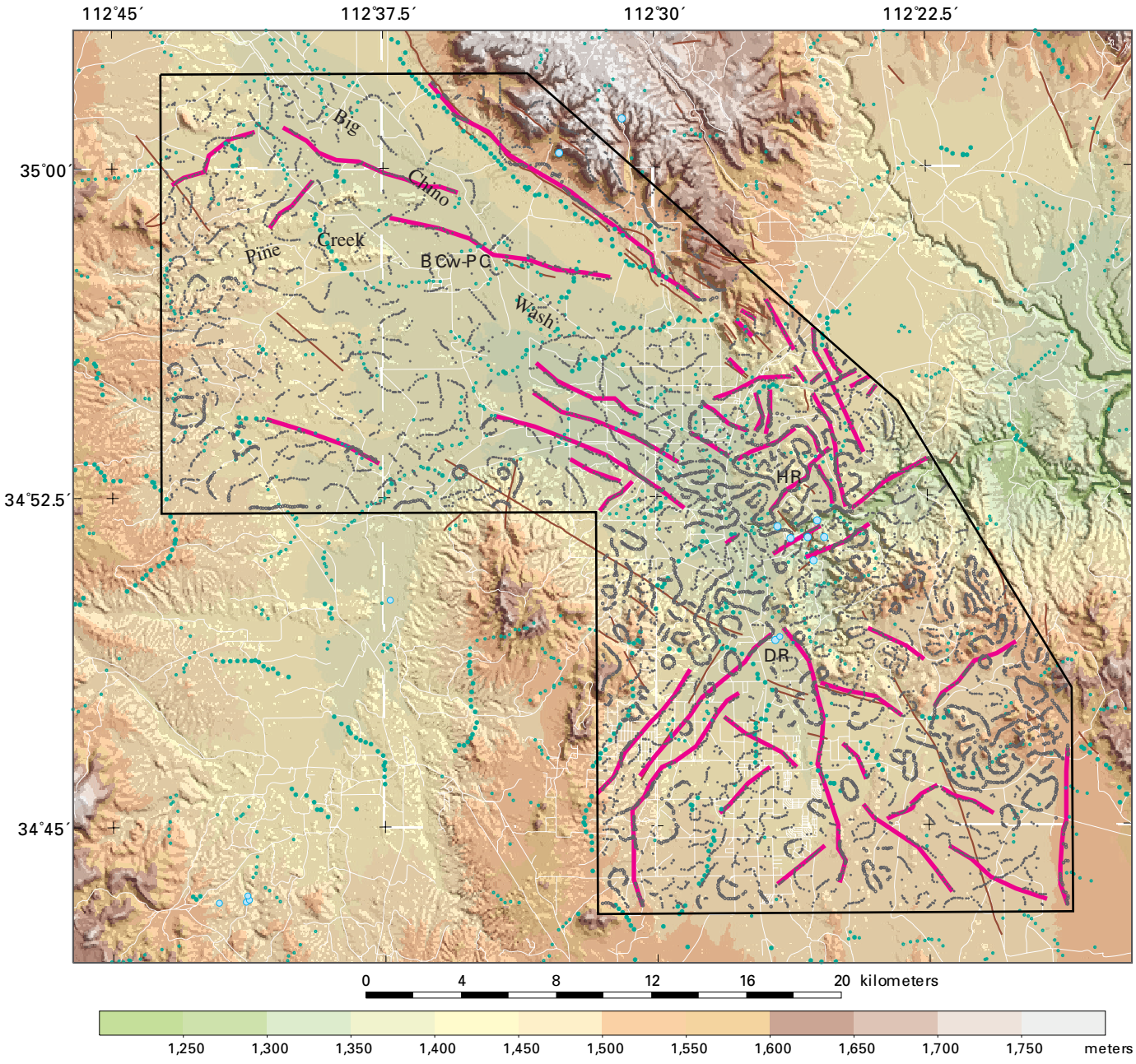

Figure C9. Map of density (green) and magnetic (gray) boundaries. Smaller dots reflect weaker gradients in gravity or magnetic data than those shown by larger dots. Magenta lines are inferred major magnetic lineaments. Magnetic lineament marked "BCw-PC" is nearly coincident with a dashed fault scarp near the junction of Big Chino wash and Pine Creek. Note that Del Rio Springs (DR) is located at the intersection of two magnetic lineaments. Brown lines are faults from this study. Blue circles are springs. HR, Headwaters Ranch area.

summarizes the magnetic susceptibility and density data of various rock types collected for this study.

The most magnetic rock types are Tertiary basalt and Tertiary lati-andesite, with average magnetic susceptibilities of 1.20 and 0.74 x 10^{-3} cgs units, respectively. The lati-andesites have the widest range in magnetic properties, ranging from 0.04 x 10^{-3} cgs units for oxidized lati-andesites to 5.04 x 10^{-3} cgs units for a Tertiary hornblende-bearing latite.

Limited physical property data related to Tertiary sedimentary rocks (4 samples) suggest that these rocks can produce measurable magnetic anomalies, although their average susceptibility is 0.26 x 10^{-3} cgs units, which is considerably less than those of the Tertiary basalt and lati-andesite. Detritus from the volcanic rocks probably is responsible for the magnetic properties of the sedimentary rocks. The most magnetic Tertiary sedimentary sample was breccia primarily composed of lati-andesite.

because of their age (more likely for the original remanence to have decayed) and grain size (coarser grain sizes indicating that original remanence may have been subjected to greater thermal changes; Tarling, 1983). Individual basalt flows in the Verde River region may have a uniform direction of magnetization, either of normal or reversed polarity (McKee and Elston, 1980). Steeply dipping faults that offset subhorizontal units, such as basalt flows, often produce magnetic anomalies that appear as linear trends on aeromagnetic maps (for example, Bath and Jahren, 1984, for the Yucca Mountain region, Nevada). The lati-andesites, on the other hand, often are extruded from volcanic plugs and thus tend to produce intense, somewhat circular magnetic anomalies. For this study, the magnetic remanence of a lati-andesite exposed in the Sullivan Buttes area was measured; its direction is reversed (declination (D) of 149° and inclination (I) of –58°; note present-day direction has D=13° and I=61°) and the intensity of the remanent magnetization is about 3x10^{-6} emu/cm^3. This information

Table C1. Densities (grams/cubic centimeter) and magnetic susceptibilites (10^{-3} cgs units) of hand samples collected for this study

[±, standard deviation; n, number of samples]

Rock Type	Density Range	Average Density	Susceptibility Range	Average Susceptibility
Tertiary basalt	2.59—2.97	2.78±0.10 (n=24)	0.14—3.98	1.20±0.99 (n=24)
Tertiary sedimentary rocks	2.35—2.57	2.46 (n=2)	0.16—0.32	0.26±0.07 (n=4)
Tertiary lati-andesite	2.27—2.91	2.59±.13(n=20)	0.04—5.04	0.74±1.05 (n=20)
Paleozoic sedimentary rocks	2.45—2.84	2.67±0.13(n=15)	0.00—0.00	0.00 (n=10)
Proterozoic rocks	2.59—3.06	2.73±0.12(n=26)	0.00—0.95	0.15±0.26 (n=41)

The magnetic properties of the Paleozoic sedimentary rocks (table C1), consisting of the Redwall Limestone, Martin Formation, and Tapeats Sandstone, are usually weak, resulting in low-amplitude magnetic anomalies generally undetectable by airborne surveys. Proterozoic rocks have a range of measured susceptibilities from 0 to 0.95 x 10^{-3} cgs units; metasedimentary rocks, such as the Mazatzal quartzite (0 x 10^{-3} cgs units), generally are incapable of producing detectable magnetic anomalies. However, metavolcanic rocks, gabbros, and some intrusive rocks can produce prominent magnetic anomalies. In the study area and vicinity, Prescott granodiorite (0.95 x 10^{-3} cgs units) and Chino Valley granite (0.88 x 10^{-3} cgs units; exposed just north of the survey area) have the highest magnetic susceptibility values of the intrusive rocks.

Magnetic susceptibility is one part of the total magnetization of a rock (as mentioned above) and primarily is a function of the amount of magnetite in the rock. The other component, the remnant magnetization, is determined by the direction and strength of the Earth's magnetic field when the rock acquired its magnetization. It can be an important component of the magnetization of the Tertiary volcanic rocks, but is unlikely to contribute to the magnetization of the Precambrian rock types

supports the interpretation that many of the circular magnetic lows in figures C2, C4, C5, and C6 are caused by reversely magnetized lati-andesite plugs.

The density measurements of this study (table C1) are consistent with earlier data (Cunion, 1985; Frank, 1984). Proterozoic rocks are dense (approximately 2.73 grams/cubic centimeter (g/cm^3)), but exhibit a wide range in values. For instance, gabbro and metavolcanic rocks are very dense (2.75 to 3.06 g/cm^3); however, representative density values of aplites and pegmatites are low (2.59 g/cm^3). The metasedimentary and granitic rocks are characterized by intermediate densities. The density of the Paleozoic rocks is indistinguishable from those of the Proterozoic granitic rocks, although the carbonate lithologies (Martin Formation and Redwall Limestone) are denser than the Tapeats Sandstone (2.62—2.84 g/cm^3 versus 2.45—2.49 g/cm^3, respectively). Similarly, the Tertiary basalts may be difficult to distinguish from the pre-Cenozoic rocks, with an average density of 2.78 g/cm^3. The lati-andesites are less dense (average 2.59 g/cm^3), although densities of vesicular basalts in the study area are as low as the average lati-andesite density.

Only two direct density measurements of the Tertiary sedimentary sequence were made in the study area; these measurements are undoubtedly biased towards higher densities because of the difficulty in obtaining a hand sample in unconsolidated materials. They are significantly less dense (~2.46 g/cm^3) than most of the other rock types. No measurements were made on Quaternary sedimentary deposits for this study. Because of the difficulty of obtaining direct density measurements on Quaternary and Tertiary sedimentary rocks, one must rely on indirect information.

Indirect information on densities of Tertiary sedimentary rocks comes from sonic velocities measured in the Bureau of Reclamation drill holes (Ostenaa and others, 1993). Using the relation of Gardner and others (1974) developed for sedimentary rocks,

$$\rho=0.23v^{0.25} \quad (1)$$

one can estimate the density, ρ (g/cm^3), from the sonic velocity, v (feet/second or ft/s). Sonic velocities measured on Quaternary and Tertiary sedimentary rocks in drillhole CV-DH-1 (Ostenaa and others, 1993) average from about 1.8 kilometers/second (km/s; 6,000 ft/s) between depths of 240-300 meters (800—1,000 feet) to as high as 3.7 km/s (12,000 ft/s) between depths of 380—410 meters (1,250—1,350 feet). In drillhole CV-DH-2, average velocities increase from 2.4 km/s (8,000 ft/s) at depths of 100—150 meters (320-500 feet) to as high as 4.9 km/s (16,000 ft/s) near the bottom of the hole. Corresponding densities for the young sedimentary deposits range from 2.02 to 2.59 g/cm^3, averaging about 2.24 g/cm^3 from 90—168 meters (300—550 feet) for CV-DH-2 and 2.20 g/cm^3 from 240-460 meters (800—1,520 feet) for CV-DH-1. Unfortunately, the deepest well studied by Ostenaa and others (1993), CV-DH-3, was not logged for velocity, although all three were logged for resistivity.

Another indirect method to estimate density is to calculate velocity from the resistivity and then use the empirical relationship shown in equation (1). All three physical properties—density, velocity, and true resistivity—are linked by a common dependence on porosity. Limitations to use of this method are described in Faust (1953). If the apparent resistivity (R_a) measured in the wells approximates the true resistivity of the rock, then Faust's (1953) empirical relationship between velocity (v) and apparent resistivity (R_a) and depth (Z) can be written

$$v=\delta(Z*R_a)^{0.1667} \quad (2)$$

where δ is an empirical constant (1948), which is applicable to most geologic sections. Using equation (1) and equation (2), average densities for the depth ranges discussed above for drillholes CV-DH-1 and CV-DH-2 are about 2.27 g/cm^3 and 2.20 g/cm^3, respectively. For CV-DH-3, densities based on this method range from 2.01 g/cm to 2.31 g/cm, but average about 2.10 g/cm^3 for depths of 61-213 meters (200—700 feet), 2.05 g/cm^3 for 213—396 meters (700 to 1,300 feet), and 2.27 g/cm^3 for 396—640 meters (1,300 to 2,100 feet).

Perhaps a better, more direct measure of the density of the sedimentary sequence comes from borehole gravity surveys outside the study area (Tucci and others, 1982). Densities derived from borehole gravity data probably are more representative of the basin rock and sediment densities because the method measures a larger volume than that of isolated hand samples or borehole velocity and resistivity logs. Another advantage of the method is that it can measure density at different depths beneath the ground surface. The mean densities from borehole gravity surveys from several scattered localities in Arizona range from approximately 1.97 to 2.32 g/cm^3 for the upper 366 meters (1,200 feet) of basin-fill deposits (Tucci and others, 1982; *their* figure 3). Figure C10 summarizes average densities derived from these various methods for Quaternary and Tertiary sedimentary rocks.

Geophysical Anomalies

The aeromagnetic anomaly patterns over Little and Big Chino Valleys (fig. C2) differ. Little Chino Valley is characterized by short-wavelength magnetic anomalies. The magnetic anomalies in Big Chino Valley tend to be broader and smoother. Little Chino Valley (except for its southwestern quarter) generally has lower magnetic values (less than 0 nT) than those over Big Chino Valley (more than 0 nT). This difference is clearly expressed in the pseudogravity field (fig. C8) and occurs roughly in the area of the Verde River canyon east of Paulden. Higher values typically occur north of the River (see for example, fig. C2, C4b, C8). The lower magnetic values in Little Chino Valley are likely caused by less magnetic Proterozoic basement (as suggested by fig. C4b and fig. C8 if these maps truly reflect deeper sources in the Proterozoic basement). Tertiary volcanic rocks, exposed or shallowly buried (< 1 kilometer), are the source of many of the very high-amplitude, short-wavelength anomalies in much of Little Chino Valley, the area around Paulden and near Sullivan Buttes. Many of the Tertiary lati-andesites coincide with very strong circular magnetic lows indicative of volcanic plugs. Tertiary basalts generally produce a "worm-like" magnetic anomaly pattern ("A" on Fig. C2). The broader, longer-wavelength anomalies in Big Chino Valley likely express deeper sources. A prominent magnetic high coincides with Paleozoic carbonate rocks exposed on Big Black Mesa (fig. C2). Because these rocks are weakly magnetic, the source of the anomaly most likely is concealed Proterozoic granitic rocks exposed just northwest of the study area. The magnetic basement on Big Black Mesa is buried by as much as 260—280 meters based on the average unit thicknesses of the Paleozoic sedimentary sequence exposed there. Sources of broader magnetic highs in the adjacent Big Chino Valley probably express Proterozoic granitic rocks deeply buried beneath the valley fill. In contrast, the Proterozoic basement beneath much of Little Chino Valley probably is metavolcanic and metasedimentary rocks, which apparently are less magnetic than the granite underlying much of Big Chino Valley and Big Black Mesa. For example, the area of exposed Proterozoic Mazatzal quartzite is a magnetically quiet region ("Xq" on fig. C5) with lower magnetic values (fig. C2).

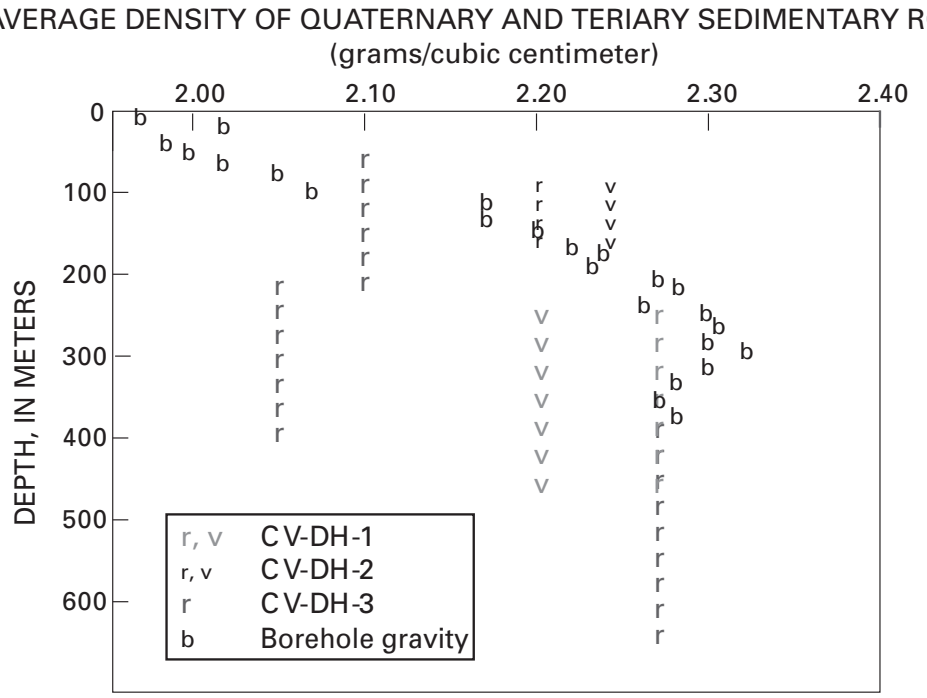

Figure C10. Average densities of Quaternary and Tertiary sedimentary rocks derived from various methods. r, derived from resistivity; v, derived from velocity; b, from borehole gravity of Tucci and others (1982; *their* figure 3).

Big Chino Valley, characterized by a gravity low, is bounded on the east by the Big Chino Fault (fig. C3). The deepest part of the basin, as suggested by the lowest gravity value within the valley, is about 5 kilometers south of the northern boundary of the study area. Gravity values increase to the southeast towards Sullivan Lake, indicating thinning of the basin-fill deposits.

Little Chino Valley is characterized by higher gravity values than those over Big Chino Valley, suggesting that Little Chino Valley basin is not as deep. South of the study area near the intersection of Highway 89 and alternate route 89 (fig. C1), a gravity low most likely reflects a thick stock of Prescott granodiorite rather than a deep basin (Cunion, 1985). The northern margin of this low is along the southern margin of the study area (fig. C3). Prescott granodiorite (and Granite Dells granite) is less dense than the some of the more mafic metavolcanic and gabbros within Proterozoic basement. This low may mask more subtle gravity lows caused by locally thick accumulations of basin fill (for example, "L" on fig. C3). Because the gravity field is affected both by changes in thickness of the Cenozoic deposits and density variations in the underlying Paleozoic and Proterozoic rocks, a method described below attempts to separate these two sources.

Depth to Basement Method

In this section, depth to pre-Cenozoic bedrock is calculated for Big Chino Valley and Little Chino Valley and to determine the geometry of bounding and internal faults.

The method used in this study to estimate the thickness of Cenozoic rocks was developed by Jachens and Moring (1990) and modified to incorporate drill hole and other geophysical data (Bruce Chuchel, U.S. Geological Survey, written commun., 1996; fig. C11). The inversion method allows the density of bedrock to vary horizontally as needed, whereas the density of basin-filling deposits is specified by a predetermined density-depth relation. Two density-depth functions listed in table C2 were used. A first approximation of the bedrock gravity field is derived from gravity measurements made on exposed pre-Cenozoic rocks, augmented by appropriate bedrock gravity values calculated at sites where depth to bedrock is known. This approximation (which ignores the gravity effects of nearby basins) is subtracted from the observed gravity, which provides a first approximation of the basin gravity field. Repeating the process using the specified density-depth relation, the thickness of the basin-fill deposits is calculated. The gravitational effect of this first approximation of the basin-fill layer is computed at each known bedrock station. This effect is, in turn, subtracted from the first approximation

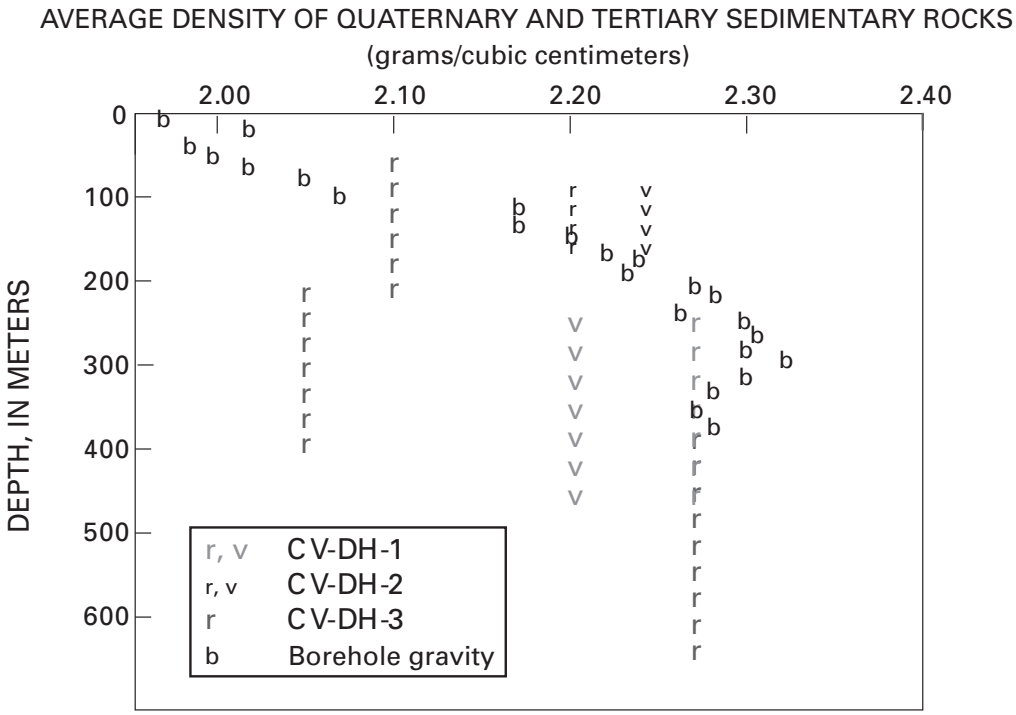

Figure C11. Schematic representation of basin-basement separation.

of the bedrock gravity field and the process is repeated until successive iterations produce no substantial changes in the bedrock gravity field.

The inversion presented here does not take into account lateral variations in the density of Cenozoic deposits, which may be an important source of error in the study area, particularly where it is underlain by thick, dense basalt flows.

Table C2. Density-depth function.*

Depth Range	Based on Arizona Borehole Gravity	Determined from Resistivity
0—100 meters	–0.67	–0.57
100—200 meters	–0.47	–0.60
200—600 meters	–0.37	–0.47
>600 meters	–0.25	–0.25

*density contrast (g/cm^3) relative to underlying pre-Cenozoic bedrock

This method has been shown to be effective in determining the general configuration of the pre-Cenozoic bedrock surface in Nevada (Phelps and others, 1999). Phelps and others (1999) showed that the model bedrock surface of Yucca Flat (Nevada Test Site, northwest of Las Vegas, Nev.) was a reasonable approximation of the true surface based on comparison with calculated basin depths from closely spaced drill holes. The predicted shape of the basin did not change significantly with additional well control. Furthermore, it seems that lateral variations in basin density, unless abrupt, do not change the overall modeled shape of the basin. Although the method is a good tool for predicting the shapes of basins, it can be less effective in estimating the magnitude of basin thickness, especially in basins containing thick basalt flows or in areas of poor well control. Below is a discussion of the sources of error in the depth-to-basement calculations.

Results

Depth to Basement

Two basin models (fig. C12) were created using two different density-depth functions (table C2). Figure C12a shows the basin model using a density-depth function based on data from Tucci and others (1982); figure C12b is the basin model using a density-depth function based on the resistivities measured in the Bureau of Reclamation drill holes (Ostenaa

and others, 1993). Because of the wide density range of the local Cenozoic volcanic rocks and their limited thickness (basalts generally less than 30 meters thick), the same density-depth relationship was assumed for Cenozoic volcanic rocks as for the Cenozoic sedimentary deposits. One might consider including the basalts with the pre-Cenozoic bedrock, but the difficulty of distinguishing dense basalt from lower-density lati-andesite in driller's logs and the presence of gravel beneath both the basalts and lati-andesites made this approach intractable. The models utilize bedrock gravity stations and well data to constrain the thickness of Cenozoic sediment.

The models were tested by comparing the predicted basin thickness with the minimum thickness of Cenozoic deposits found in wells that did not bottom in pre-Cenozoic rock (fig. C13). In Big Chino Valley, the basin thickness predicted by the models generally is greater than that found in these wells (fig. C13; pink areas are where model thickness is supported by these wells). In Little Chino Valley, the basin models agree with the well data in the central part of the valley, where the deepest part of the basin is modeled and where the lowest isostatic gravity values ("L" on fig. C3) are located. Along the western margin of the valley where wells did not encounter pre-Cenozoic rock, the models underestimate basin-fill thickness by as much as 250 meters. The western part of the valley coincides with a large positive gravity anomaly (fig. C3, C7; dashed gray line on fig. C13). Without well control to constrain the bedrock gravity, the modeling process will not show a basin in the vicinity of the gravity high. Another substantial underestimate of basin fill (269 meters or 881 feet) is 3 kilometers east of the deepest part of the Little Chino Valley basin, where the thickest Tertiary volcanic rock was encountered in drillholes. The basin model using the density-depth function based on Tucci and others (1982) produces fewer underestimates in Little Chino Valley. However, both models are poorly constrained in Little Chino Valley because of the limited wells that penetrate pre-Cenozoic rock (thus constraining the bedrock gravity component; see fig. C14) and because of the thickness of volcanic rock within the sediments (resulting in inaccurate density-depth functions and possibly in substantial lateral variations in the density of rock and sediment units).

The basin models appear to be more accurate for Big Chino Valley, even though wells that bottomed in pre-Cenozoic rock are limited to its southern margin. The northernmost wells that penetrated pre-Cenozoic bedrock (CV-DH-1 and CV-DH-2) did not encounter Tertiary volcanic rock. Northwest-trending magnetic anomalies (fig. C2) suggest that the Tertiary basalt deepens to the northwest from exposures near Paulden and terminates southeast of these two drill holes. Thus, the presence of shallowly buried, thick basalt flows, which can introduce error in the inversion method, is unlikely in the central part of Big Chino Valley. No information on bedrock gravity variations is available for central Big Chino Valley, but bedrock gravity values at CV-DH-1 and CV-DH-2 are comparable to those measured on Big Black Mesa (fig. C14). The lack of evidence for significant variations in bedrock gravity could indicate similar basement rock beneath Big Chino Valley and Big Black Mesa. The aeromagnetic data suggest that the magnetic basement of Big Black Mesa does extend southwest of the Big Chino fault (fig. C2, fig. C4), at least as far as the scarp near the intersection of Big Chino Wash and Pine Creek (BCw-PC on fig. C9). Thus, large variation in bedrock density is not anticipated at least beneath the eastern part of Big Chino Valley.

Another test of the basin model is a comparison of the basin depths with those predicted from resistivity depth soundings (Ostenaa and others,1993; Water Resources Associates, 1989). Of the 19 soundings within the study area (Ostenaa and others, 1993), only 2 soundings (Z7 and Z10) disagree substantially with the basin models (depths to Paleozoic rock from resistivity, 600 and 780 meters, depths predicted by basin models, 1,100 and 1,400 meters). These soundings flanking CV-DH-3 lie in the deeper part of the basin. The modeled resistivities interpreted as Paleozoic rock at these two sites are indistinguishable from resistivities measured at the bottom of CV-DH-3, which encountered Tertiary lati-andesite, suggesting that the resistivity method may not be capable of distinguishing Paleozoic rock from Tertiary lati-andesite. The depth soundings presented in Water Resources Associates (1989) are all consistent with basement depths estimated by the gravity inversion method. Thus, the basin models predicted from the gravity inversion are in substantial agreement with the resistivity soundings.

Another test of the basin model was made after the models were created; deep wells in Big Chino, Little Chino, and Williamson Valleys were completed and reached bedrock. In all cases, the predicted basin depths within the study area were deeper than the depths at which bedrock was encountered. Two of the wells drilled in Big Chino Valley (fig. C12; CVR-1, bedrock at 149 meters; CVR-2, bedrock at 494 meters) agree within 1-21 percent of the predicted basin depths (resistivity model, 179 and 500 meters; Tucci model, 181 and 563 meters, respectively). The third well (fig. C12; CVR-3) penetrated bedrock substantially above both of the predicted basin thicknesses (512 meters versus 1,224 and 1,444 meters). One well in Little Chino Valley (16N/1W/23aca) hit bedrock at a depth of 148 meters, within 25 percent of the predicted basin depths (both 185 m). Two deep wells (fig. C12) were drilled in the Williamson Valley, outside of the study area. One well within the gravity low did not penetrate basement at a depth of 457 meters (BH-1), which is consistent with the predicted basin thicknesses. The well outside the gravity low (BH-3) penetrated bedrock at a depth of 429 meters. The basin depth calculated with the resistivity derived density-depth function (569 meters) was closer to the actual bedrock surface than the basin depth calculated with the Tucci density-depth function (755 meters). The consistent overestimation of basin thickness by the models at wells that did penetrate bedrock suggests that a lighter density-depth function should be used for future work, especially for Big Chino and Williamson Valleys.

Both models show similar shapes for the basin configuration in the study area, but predict slightly different thicknesses. For example, at CV-DH-3, the modeled basin depth

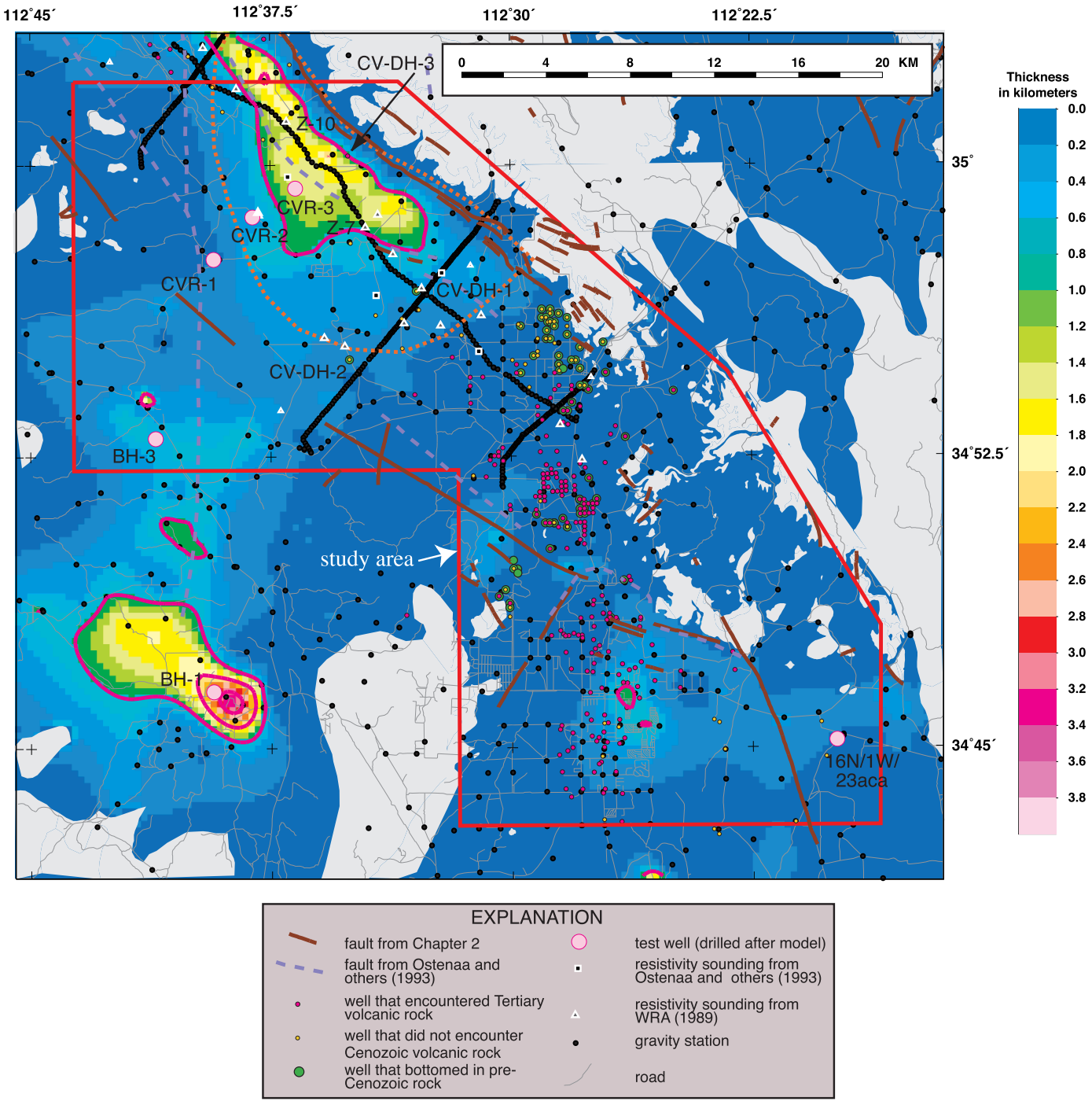

Figure C12a. Map of modeled thickness of Cenozoic sedimentary and volcanic fill using the density-depth function of Tucci and others (1982). Thick magenta lines are 1-kilometer contours. Dashed orange line outlines extent of playa deposit from Schwab (1995). Pale gray areas are pre-Cenozoic outcrops.

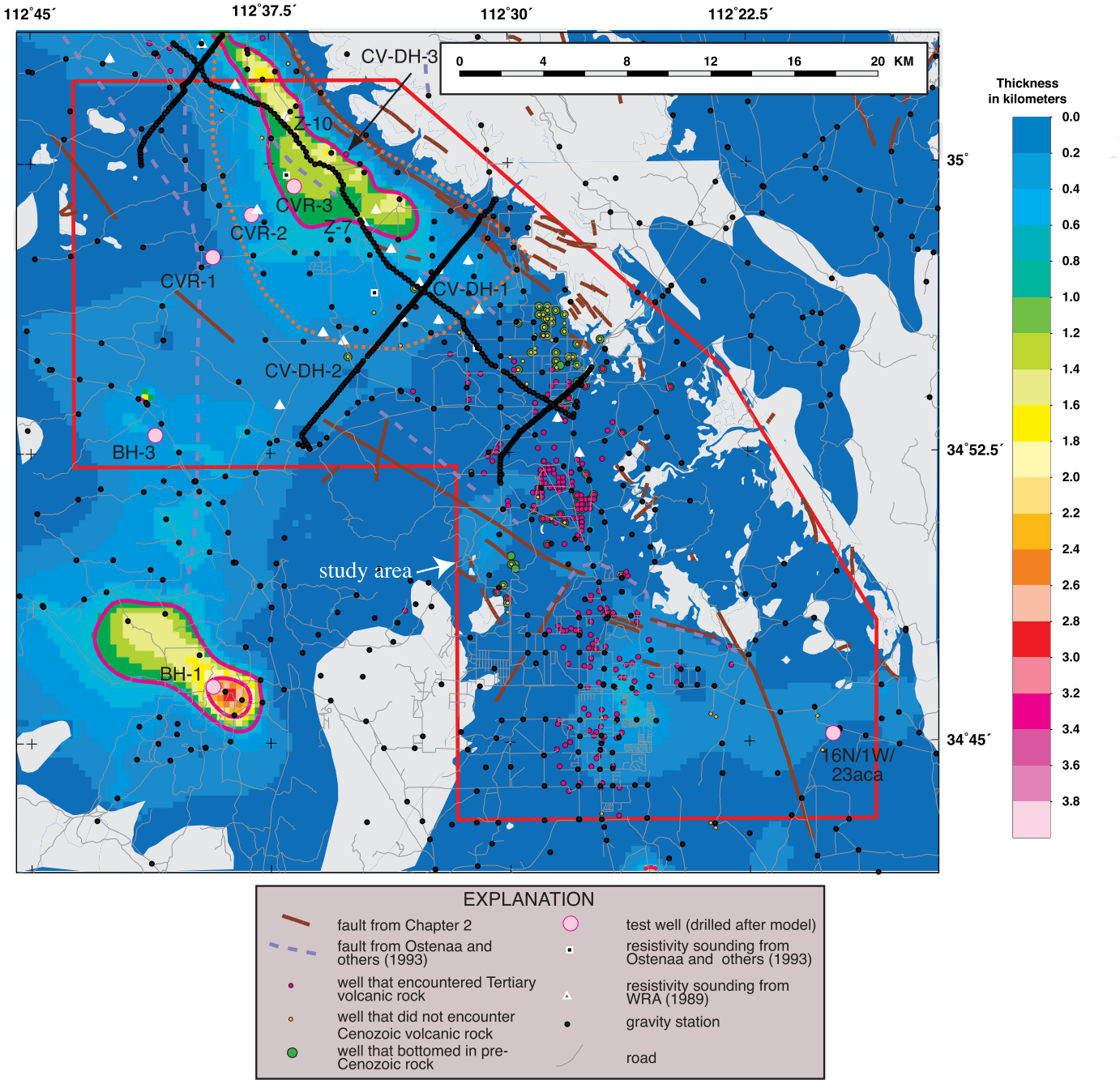

Figure C12b. Map of modeled thickness of Cenozoic sedimentary and volcanic fill using a density-depth function derived from resistivity logs. Thick magenta lines are 1-kilometer contours. Dashed orange line outlines extent of playa deposit from Schwab (1995). Pale gray areas are pre-Cenozoic outcrops.

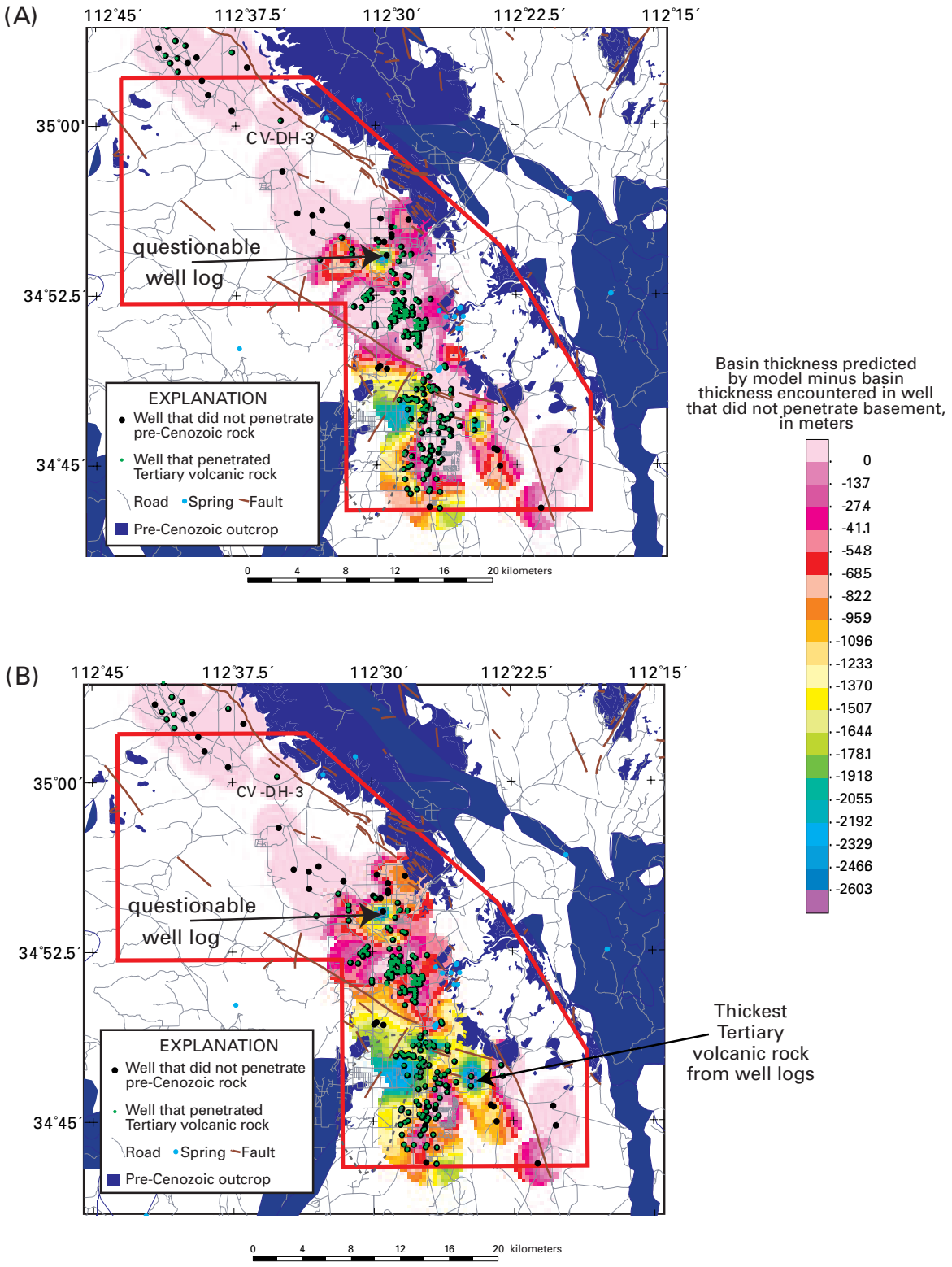

Figure C13. Maps of mismatch between basin thickness encountered in wells that did not encounter pre-Cenozoic bedrock and predicted basin thickness from gravity inversion models. Thick red line is survey boundary. Gray dashed line shows extent of gravity high. White areas are basin areas that do not have wells. Pink areas are where basin model thickness agrees with thickness encountered by well. Questionable well log is inconsistent with geology interpreted from adjacent well logs. *(A)* Mismatch for model using Tucci and others (1982) density-depth function. *(B)* Mismatch for model using density-depth function based on resistivity.

is 1 kilometer in figure C12a, but about 800 meters in figure C12b. CV-DH-3 bottomed in 50 meters (165 feet) of "basalt" (lati-andesite; Chapter B) at a depth of 748 meters (2455 feet). The basin models suggest that there is another 50—250 meters of Cenozoic volcanic (and presumably sedimentary) deposits below the bottom of the drill hole. Because lati-andesite underlain by Tertiary gravel is exposed on the upthrown side of the Big Chino fault on South Butte (approximately 10 kilometers northwest of the northeast corner of the aeromagnetic survey) gravel most likely underlies the lati-andesite at CV-DH-3.

The thickness of the gravel on the downthrown block could be greater than that of the upthrown block if a substantial portion of the topographic relief associated with Big Black Mesa existed at the time of gravel deposition, as inferred by Ostenaa and others (1993). The gravity inversion models suggest an additional thickness of gravel and lati-andesite of 50—250 meters beneath the bottom of CV-DH-3; the lower bound is consistent with geologic inference (Chapter B).

Estimates of the total sediment volume for the two models for the area of Big Chino Valley within the study area

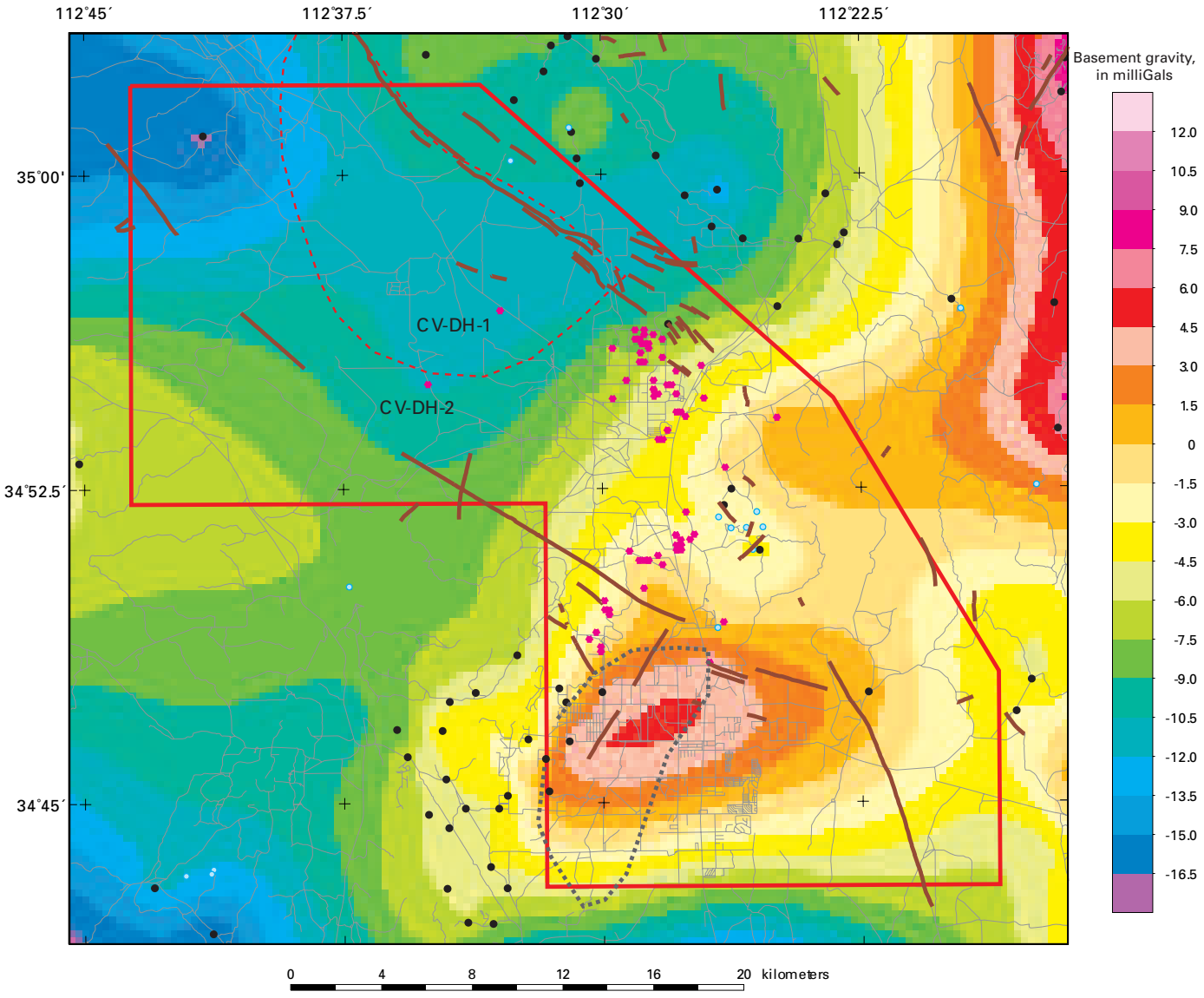

Figure C14. Basement gravity map (Model 2 based on density-depth function from resistivity). Black circles are gravity stations measured on bedrock. Magenta circles are wells that encountered bedrock. Gray dotted line outlines extent of isostatic gravity high that underlies western part of Little Chino Valley. The gravity inversion shows a basement gravity high in roughly the same area, but poorly matches the orientation of the high. This mismatch will introduce error in the basin thickness model. Alternatively, the source of the gravity high could reflect a great thickness of Tertiary high-density basalts within the fill (representing a large lateral change in basin-fill density that is not accounted for in the basin inversion method).

range from 140.2 to 158.4 cubic kilometers (1.14 to 1.29 x 10^8 acre-feet). The models show the basin beneath Big Chino Valley as asymmetric, with the deepest part of the basin along the northeastern margin of the valley and generally elongated parallel to the trend of the Big Chino fault. The deepest part of the basin is 3—4 kilometers wide; however, the western margin of the basin in the central part of the valley is not well defined because of the paucity of gravity stations. Detailed gravity profiles are limited to only the extreme northern and southern ends of the basin (fig. C3, C12). Thus, the western margin (presumably fault controlled) may trend parallel to the Big Chino fault (as suggested by Ostenaa and others, 1993). Alternatively, the western margin may trend more westerly and parallel to the scarp near Big Chino Wash and its coincident magnetic edge (BCw-PC; fig. C9).

Playa Deposit/Alluvial Fans

One feature that has figured prominently in discussions concerning ground-water flow within Big Chino Valley is a deposit of fine-grained sediment in the center of the basin. The fine-grained sediments were deposited in a playa environment, formed by damming of from Big Chino Valley by basalt flows east of Paulden (Chapter B; Ostenaa and others, 1993). Preservation of the deposit may have been facilitated by downdropping of the basin by the Big Chino fault during late Tertiary and Quaternary time (Menges and Pearthree, 1983; Ostenaa and others, 1993).

The lateral extent of the playa deposit is approximately known from water well logs (Schwab, 1995; dashed orange line on fig. C3). The thickest part of the playa deposit is found in drill hole CV-DH-3 (~ 670 meters or 2,200 feet; Ostenaa and others, 1993; Chapter B). The playa deposit thickens towards the center of Big Chino Valley (Schwab, 1995; Ostenaa and others, 1993; and Chapter B). Gravity and resistivity methods may be a viable tool to map the distribution of playa deposits because fine-grained sediment is characterized by high porosities (thus low densities) and by low resistivities (less than 10 ohm-m).

A resistivity log indicates very low resistivities (as low as 1—2 ohm-m) in CV-DH-3 (Ostenaa and others, 1993, their fig. 3.A-2). Low resistivities (10 ohm or less) suggest the presence of saturated playa sediment. Resistivity depth soundings 3—4 kilometers northwest and southeast of the drillhole show higher resistivities. Part of this difference between the logged resistivities in CV-DH-3 and adjacent soundings can be attributed to the limited area probed by the logging method, possible contamination by drilling fluids, or irregularities on the bore surface. In other studies, a comparison of soundings derived from well logs and coincident sounding data often shows similar curves, but the log resistivities are 25 to 40 percent lower than the sounding data (R. Bisdorf, USGS, written commun., 2001). Adjusting the log resistivities at CV-DH-3 produces resistivities of less than 10 ohm-m. A resistivity profile along the southern margin of the basin, perpendicular to the axis of the valley, indicates resistivities of l0 ohm-m or less near the eastern margin of the valley (Ostenaa and others, 1993, their fig. 3.A-3).

The resistivity soundings are limited areally as are the wells used by Schwab (1995) to delineate the outline of the playa (dashed orange line on fig. C3). Because density and resistivity are linked by a dependence on porosity, the gravity field may be useful in mapping the extent of the playa deposit. The extent of the playa deposit (fig. C3) matches much of the gravity low of Big Chino Valley. Gravity data filtered to enhance shallow sources, such as those within the basin, show low values concentrated along the eastern margin of the basin (fig. C7). Assuming that these anomalies reflect high-porosity basin fill, then one can map thickness variations in the fill. Thus, the basin thickness models can serve as a proxy for the thickness of the playa deposit, assuming that the deposit is continuous throughout the basin between depths of 100 and 700 meters (the depth range of playa deposit encountered in CV-DH-3). However, the gravity inversion method does not have the resolution to map thin lenses of gravel within the deposit, and fails to account for possible lateral variations in density within the basin (for example, coarse-grained alluvial fan deposits that lie adjacent to the Big Chino fault). Note, however, that if coarse-grained deposits are present along the fault zone, they are restricted to less than 1 or 2 kilometers southwest of the fault zone (see Ostenaa and others, 1993, their cross-section F-F'). Gravity models constrained by CV-DH-3 do not indicate a large volume of dense, coarse-grained deposits between CV-DH-3 and the Big Chino fault. However, these models provide nonunique answers. A multitude of geometries can produce the same observed gravity anomaly. Resistivity or high-resolution seismic surveys that cross the fault may help define the dimensions of lens-shaped or thin bodies of coarse-grained deposits along the fault zone and possibly within the playa deposit.

Distribution of Volcanic Rocks in Subsurface

Magnetic anomalies reflect the presence of magnetic rock types within Tertiary volcanic rock and Proterozoic basement. Exposed volcanic rock produces either "wormlike" or semicircular anomaly patterns, as delineated by the magnetic boundaries on Figures C9 and C15. The magnetic boundaries often coincide with topographic relief on the volcanic rock, shown as dark blue lines on figure C15. Semicircular anomalies characterize exposed Tertiary lati-andesite; the anomalies usually are intense magnetic lows indicating reversely magnetized rock. Semicircular magnetic lows over areas covered by young sedimentary deposits are probably Tertiary lati-andesite plugs (annotated with "p" on fig. C15). Some of the semicircular magnetic highs ("p+") also could be caused by lati-andesite plugs that are normally polarized or by semicircular hills of normally polarized basalt (see "b?" on fig. C15). A magnetic high at Table Mountain in the extreme southwest corner of the study area coincides with lati-andesite. A corresponding radiogenic anomaly rules out interpretation as a mafic rock such as basalt or metagabbro; see Chapter B. A circular magnetic high

1.5 kilometers north-northeast of Table Mountain also could indicate lati-andesite; alternatively, the source of the positive anomaly could be Proterozoic basement or Tertiary basalt. Tertiary basalt and Proterozoic basement are exposed immediately south of the survey boundary 2 kilometers east of Table Mountain (Krieger, 1965; Billingsley and others, 1988).

Exposed Tertiary basalt (Tby on fig. C15) produces a complicated "wormlike" magnetic anomaly pattern. In the area east of Paulden and immediately north of the Verde River, exposed basalt produces high-frequency magnetic anomalies. Some magnetic boundaries associated with the Tertiary basalt coincide with topographic relief of the exposed basaltic surface; others coincide with the contact of the basalt with weakly magnetic Paleozoic limestone. The basalt seems to be reversely polarized in the Headwaters Ranch area (HR on fig. C9), where exposed limestone coincides with a magnetic high and the surrounding basalt coincides with pronounced magnetic lows. The magnetic high is caused by the underlying Proterozoic basement (possibly granite similar to that beneath Big Black Mesa). The basalt has been dated at 4.5 Ma (McKee and Anderson, 1971) and according to the magnetostratigraphic timescale (Harland and others, 1982), should be reversely polarized. Water well logs indicate that the basalt is 148 meters (485 feet) thick about 1 kilometer north of the limestone outcrop and within the magnetic low. The increase in thickness of the basalt from 0 meters at the limestone to 148 meters at HR-2 (Ostenaa and others, 1993, their table F) would produce a negative magnetic anomaly if the basalt were predominantly reversely polarized. This change in thickness may reflect a buried fault (with a northeast strike) or topography on the pre-basalt surface (such as a paleochannel). The magnetic boundaries elsewhere within this magnetically complicated area may thus reflect abrupt changes in thickness of the basalt. The variations in thickness of basalt could have resulted from flow around topographic features produced by erosion, faulting/fracturing, or a combination of both (light blue lines on fig. C15). Other explanations for the complicated variations in the magnetic field include relief on the Proterozoic surface and variations in magnetization within either the basalt or Proterozoic basement. Without more physical property information, deeper drill holes with reliable logs, and hydrologic data, one can only point to these areas marked by strong magnetic boundaries as potential sites underlain by fractures, faults, or channel margins that likely influence the movement of ground water in this area.

West and northwest of the exposed basalt in the Verde River gorge area, strong magnetic boundaries over young sedimentary deposits (units Qal and Qs on fig. C15) may be extensions of those over exposed basalt. Well logs indicate shallow volcanic rock (generally less than 50 meters deep). About 4 kilometers northwest of the exposures of Tertiary basalt, the magnetic anomalies are less intense and strike predominantly northwest (parallel to the Big Chino fault; fig. C2, C5). Wells (150 meters or deeper) bottom in Tertiary volcanic rock in this area. Relief on the upper surface of the volcanic rock probably is the source of these northwest-striking anomalies. The anomalies and, thus, the basalt cannot be traced more than 10 kilometers northwest from outcrops (red line on fig. C5). Thus, these northwest-striking magnetic boundaries most likely delineate faults that offset the volcanic rock or channelways (also probably fault controlled) that the volcanic rock flowed down. Tilting of the basalt could produce these anomalies; however, evidence indicates little tilting of the basalt, and well data indicate little stratigraphic separation between basalt flows (Chapter B). These features most likely are related to faulting because their strike is parallel to the most prominent fault in the study area, the Big Chino fault.

The gravity and magnetic data in Little Chino Valley do not indicate deep basins or steeply-dipping, large-offset normal faults, in contrast to the anomaly patterns in Big Chino Valley. Nor do these data detect the presence of the horseshoe-shaped Del Rio fault as inferred by Ostenaa and others (1993), although Del Rio springs is located near the intersection of magnetic lineaments (fig. C9). Almost all of the mapped faults shown in figure C15 in Little Chino Valley cut across magnetic boundaries, suggesting that fault displacements are small (less than 100 meters). Several semicircular magnetic anomalies may express concealed lati-andesite plugs, whose tops lie 300 meters or shallower based on the method of Peters (1949). Well logs indicate that several of the plugs are buried less than 200 meters. The plugs tend to be located along the margins of the valley. The maximum calculated depth to the top of an individual plug is on the order of 700 meters, based on inspection of residual anomalies after upward continuation of the magnetic field 700 and 800 meters (the depth to the top of the lati-andesite found in CV-DH-3 in Big Chino Valley). It is possible that the relative absence of plug-related anomalies in the central part of the valley west of Granite Creek is caused by a greater depth of burial to the top of the plugs. Part of this area coincides with a local gravity low ("L" on fig. C3, C7) that has north-striking edges, the eastern edge of which corresponds with a subtle magnetic gradient. The middle part of this magnetic gradient coincides roughly with a change in water-table elevation (highlighted by dashed light blue line on fig. C15). Another north-south trending gradient in the southeastern part of the survey area (dashed light blue line on fig. C15) coincides with a large change in water-level elevation (60 to more than 120 meters or 200 to more than 400 feet depths; Arizona Department of Water Resources, 2001, written communication). The magnetic gradient overlies alluvial deposits, but the source of the anomaly probably is in Proterozoic basement. North-striking magnetic, gravity and radiometric gradients caused by exposed Proterozoic basement are 5 kilometers east of the survey boundary (Langenheim and others, 2000). Thus, magnetic and gravity lineaments, even if caused by physical property variations in Proterozoic basement, also may locate potential groundwater pathways (fractures or faults within the impermeable crystalline basement). Inferred major lineaments are shown in magenta on figures C9 and C15. The relation of ground-water flow and these lineaments, if any, needs to be determined by acquiring additional data, such as hydrologic data from existing and new wells.

Conclusions and Recommendations

The aeromagnetic and gravity data provide new insights on the distribution of and structures associated with Tertiary volcanic rock and Proterozoic basement beneath Big and Little Chino Valleys. Some of these concealed structures may act as potential pathways or barriers for groundwater movement. Of particular interest are the shallowly buried lati-andesite plugs in northern Little Chino Valley, manifested as semicircular magnetic lows. Magnetic data, as well as limited well data, indicate that these plugs lie as much as 200 to 300 meters beneath valley fill. The plugs are mostly likely barriers to ground-water flow, based on the relatively unfractured and impermeable nature of exposed intrusive centers, compared to the fractured and permeable nature of the flows and volcaniclastic aprons.

The gravity data provide additional information on basin thickness in Big Chino Valley. By using a gravity inversion method, estimates of the total sediment volume for the area of Big Chino Valley within the study area range from 140.2 to 158.4 cubic kilometers (1.14 to 1.29 x 10^8 acre-feet). Additional constraints, such as wells that penetrate the entire basin sequence in both valleys and more detailed gravity, electric or seismic surveys, would reduce uncertainty in estimates presented here. New wells also could test whether the structures identified here influence ground-water movement. For example, are northwest-trending fractures (inferred from geologic and geophysical data) more open to fluid flow, as proposed for these fractures throughout the Colorado Plateau (Thorstenson and Beard, 1998)?

References Cited

Baranov, V., 1957, A new method for interpretation of aeromagnetic maps: Pseudo-gravimetric anomalies: Geophysics, v. 22, p. 359-383.

Bath, G.D., and Jahren, C.E., 1984, Interpretations of magnetic anomalies at a potential repository site located in the Yucca Mountain area, Nevada Test Site: U.S. Geological Survey Open-File Report 82-536, 27 p.

Billingsley, G.H., Conway, C.M., and Beard, L.S., 1988, Geologic map of the Prescott 30 by 60-minute quadrangle, Arizona: U.S. Geological Survey Open-File Report 88-372, scale 1:100,000.

Blakely, R.J., 1996, Potential Theory in Gravity and Magnetic Applications: Cambridge University Press, 441 p.

Blakely, R.J., and Simpson, R.W., 1986, Approximating edges of source bodies from magnetic or gravity anomalies: Geophysics, v. 51, p. 1494-1498.

Cunion, Edward Joseph, Jr., 1985, Analysis of gravity data from the southeastern Chino Valley, Yavapai County, Arizona: Northern Arizona University Master's thesis, 110 p.

Davis, S.N., and DeWeist, R.J.M., 1966, Hydrogeology: John Wiley & Sons, p. 374-380.

Dobrin, M.B., and Savit, C.H., 1988, Introduction to Geophysical Prospecting: McGraw-Hill Book Company, 867 p.

Faust, L.Y., 1953, A velocity function including lithologic variation: Geophysics, v. 18, no. 2, p. 271–288.

Frank, A.J., 1984, Analysis of gravity data from the Picacho Butte area, Yavapai and Coconino counties, Arizona: Northern Arizona University Master's thesis, 91 p.

Gardner, G.H., Gardner, L.W., and Gregory, A.R., 1974, Formation velocity and density: the diagnostic basis for stratigraphic traps: Geophysics, v. 39, p. 770-780.

Grauch, V.J.S., and Cordell, Lindrith, 1987, Limitations of determining density or magnetic boundaries from the horizontal gradient of gravity or pseudogravity data: Geophysics, v. 52, no. 1, p. 118-121.

Harland, W. B., Cox, Allan, Llewellyn, P. G., Pickton, C. A .G., Smith, A. G., Walters, R., and Fancett, K. E., 1982, A geologic time scale: Cambridge University Press, 131 p.

Jachens, R.C., and Moring, B.C., 1990, Maps of the thickness of Cenozoic deposits and the isostatic residual gravity over basement for Nevada: U.S. Geological Survey Open-File Report 90-404, 15 p., 2 plates.

Krieger, M.H., 1965, Geology of the Prescott and Paulden quadrangles, Arizona: U.S. Geological Survey Professional Paper 467, 127 p.

Langenheim, V.E., Duval, J.S., Wirt, Laurie, and DeWitt, Ed, 2000, Preliminary report on geophysics of the Verde River headwaters region, Arizona: U.S. Geological Survey Open-File Report 00-403, 28 p. (http:// wrgis.wr.usgs.gov/open-file/of00-403).

Langenheim, V.E., and Jachens, R.C., 1996, Thickness of Cenozoic deposits and groundwater storage capacity of the westernmost part of the Las Vegas Valley, inferred from gravity data: U.S. Geological Survey Open-File Report 96-259, 29 p.

McKee, E.H., and Anderson, C.A., 1971, Age and chemistry of Tertiary volcanic rocks in north-central Arizona and relation of the rocks to the Colorado plateaus: Geological Society of America Bulletin, vol.82, no.10, p.2767-2782.

McKee, E.H., and Elston, D.P., 1980, Reversal chronology from a 7.9–11.5 m.y. old volcanic sequence in central Arizona: Comparison with ocean floor polarity record: Journal of Geophysical Research, v. 85, p. 327-337.

Menges, C.M., and Pearthree, P.A., 1983, Map of neotectonic (latest Pliocene-Quaternary) deformation in Arizona: Arizona Bureau of Geology and Mineral Technology, Open-File Report 83-22, 48 p.

Ostenaa, D.A., Schimschal, U.S., King, C.E., Wright, J.W., Furgerson, R.B., Harrel, H.C., and Throner, R.H., 1993, Big Chino Valley groundwater study: Geologic framework investigations: Bureau of Reclamation, Denver, CO, 31 p.

Peters, L.J., 1949, The direct approach to magnetic interpretation and its practical application: Geophysics, v. 14, p. 290-320.

Phelps, G.A., Langenheim, V.E., and Jachens, R.C., 1999, Thickness of Cenozoic deposits of Yucca Flat inferred from gravity data, Nevada Test Site, Nevada: U.S. Geological Survey Open-File Report 99-310, 33 p.

Phillips, J.D., 2001, Designing matched bandpass and azimuthal filters for the separation of potential-field anomalies by source region and source type: Australian Society of Exploration Geophysicists, 15th Geophysical Conference and Exhibition, Expanded Abstracts CD-ROM, 4 p.

Schwab, K.J., 1995, Maps showing groundwater conditions in the Big Chino Sub-Valley of the Verde River valley, Coconino and Yavapai counties, Arizona—1992: Department of Water Resources, Hydrologic Map Series Report Number 28, Phoenix, Arizona, 1 sheet.

Simpson, R.W., Jachens, R.C., Blakely, R.J., and Saltus, R.W., 1986, A new isostatic residual gravity map of the conterminous United States with a discussion on the significance of isostatic residual anomalies: Journal of Geophysical Research, v. 91, p. 8348-8372.

Tarling, D.H., 1983, Paleomagnetism: Principles and Applications in Geology, Geophysics, and Archaeology: Chapman and Hall, Ltd: New York, 379 p.

Thorstenson, D.J., and Beard, L.S., 1998, Geology and fracture analysis of Camp Navajo, Arizona Army National Guard, Arizona: U.S. Geological Survey Open-File Report 98-242, 42 p.

Tucci, Patrick., Schmoker, J.W., and Robbins, S.L., 1982, Borehole-gravity surveys in basin-fill deposits of central and southern Arizona: U.S. Geological Survey Open-File Report 82-473, 24 p.

Water Resources Associates, Inc., 1989, Hydrogeology investigation, Big Chino Valley, Yavapai county, Arizona, Phase I, Volumes I & II: consultants reports for City of Prescott, City Attorney's Office, Prescott, Arizona, November 29, 1989, 2 volumes.

Wirt, Laurie, and Hjalmarson, H.W., 2000, Sources of springs supplying base flow to the Verde River headquarters, Yavapai County, Arizona: U.S. Geological Survey Open-File Report 99-0378, online release (*http://pubs.usgs.gov/of/1999/ofr-99-0378*), 54 p.

EXPLANATION

Quaternary

- Qal-Alluvium
- Qs-Sediment
- Qt-Terrace gravel
- Qg-Gravel
- Qf-Fanglomerate
- Qc-Colluvium
- QTs-Sedimentary rocks (Quaternary and Tertiary)
- QTf-Fanglomerate (Quaternary and Tertiary)

Tertiary

- Taby-Alkali basalt)
- Tby-Basalt (Tertiary)
- Thb-Hickey Formation
- Tlau-Lati-andesite
- Tlal-Lati-andesite
- Tov-Volcanic rocks
- Tbu-Basalt, undivided
- Tsy-Sedimentary rocks
- Tso-Sedimentary rocks
- Tos-Sedimentary rocks
- Tsu-Sedimentary rocks, undivided)

Paleozoic

- Pkt-Kaibab and Toroweap Formations (Lower Permian)
- Pc-Coconino Sandstone (Lower Permian)
- Ps-Supai Formation (Lower Permian and Upper Pennsylvanian)
- Mr-Redwall Limestone (Upper and Lower Mississippian)
- Dm-Martin Formation (Upper and Middle? Devonian)
- Ct-Tapeats Sandstone (Middle and Lower Cambrian)

Precambrian

- ZYgr-Granite (Middle? Proterozoic)
- Xq-Mazatzal Formation (early Proterozoic)
- Xkw (Xap)-Alaskite of King Wash (early Proterozoic)
- Xis-Granite of Iron Springs (early Proterozoic)
- Xu-Granitic and metamorphic rocks, undivided (early Proterozoic)
- Xt-Tuffaceous metasedimentary rocks (early Proterozoic)
- Xb-Basaltic metavolcanic rocks (early Proterozoic)